Correspondence to:

Z. Dai,
zjdai@sklec.ecnu.edu.cn

Author Contributions:

Data curation: Jie Mi
Methodology: Jie Mi
Software: Jie Mi

Morphodynamic Resilience of the Tide-Dominated Estuary With Interference From Tidal Flat Reclamations

Min Zhang[1,2], Hangxing Wu[1], Zhijun Dai[2] , Jie Mi[1], and Huayang Cai[3]

[1]School of Environmental and Geographical Sciences, Shanghai Normal University, Shanghai, China, [2]State Key Laboratory of Estuary and Coastal Research, East China Normal University, Shanghai, China, [3]School of Ocean Engineering and Technology, Sun Yat-sen University, Zhuhai, China

Abstract Most tide-dominated estuaries worldwide are among the morphodynamic shrinking types heavily disturbed by anthropogenic interventions like embankments and reclamations. A typical example is North Branch (NB), the northern first-order distributary of Yangtze (Changjiang) Estuary, showed a rapid alteration from river-dominated to tide-dominated character in less than 50 years after intensive reclamations, resulting in serious morphodynamic shrinkage, thus attracted great concern of its evolutionary fate. Here, we explored this issue based on historical bathymetry data and hydro-morphodynamic modeling to examine the morphology-hydrology interactions and the suggested equilibrium re-adjustment mechanism after intensive reclamations. Results demonstrated a mechanism of geomorphological resilience for the tide-dominated estuary, evolving from preliminary estuarine shrinking to dynamic equilibrium after reclamations. Although reclamation could destabilize the system, leading to temporary positive feedback between tidal pumping and morphology shrinking, driving the estuary vanishing quickly in a short time. A substantial loss in the intertidal areas, changing the estuary geometry from a highly-curved bank to a highly-constrained channel, weakened flood tidal asymmetry of NB, which in turn altered sediment dynamics from deposition to erosion. Such negative feedback process tends to drive the estuary toward a new dynamic equilibrium morphology. The discovered nonlinear feedback mechanism is supported by the evidence of system efficiency adjustment, which was substantially gained during the first 30 years, then stayed in a low entropy production and minimum work state, indicating a more efficient dynamic equilibrium. If further estuary preservation policies are implemented, the dynamic equilibrium of NB is expected to continue for a long time in the future.

Plain Language Summary Tide-dominated estuaries worldwide have experienced a morphological shrinking under anthropogenic reclamations. However, few researchers have explored the positive and negative feedback processes that drive the system adjustment between fast shrinking and equilibrium states, especially for a large system like North Branch (NB) in Yangtze Estuary. The results of hydro-morphodynamic modeling and system efficiency analysis showed the preliminary fast decline of NB was due to local reclamation works, but then it was transferred to a dynamic equilibrium state during the recent 20 years owing to the geomorphological resilience adjustment of the large, tide-dominated system. Although reclamation could destabilize the system, leading to temporary positive feedback between tidal pumping and morphology shrinking, a substantial loss in the intertidal areas weakened the flood tidal asymmetry, fostering negative feedback, thus can drive the estuary toward a new dynamic equilibrium morphology. The proposed geomorphological resilience adjustment mechanism of a tide-dominated system may be relevant to other estuarine and coastal areas worldwide, subject to large-scale reclamations.

1. Introduction

Most estuaries in the world were formed approximately 60 million years ago when the river valleys were drowned during the rapid post-glacial sea-level rise period (J. Chen et al., 1979; Dalrymple & Choi, 2007; S. Gao, 2013). Despite their millennial lifetime, many were heavily reclaimed in the last century, driven by either economic gain or safety purposes (Nienhuis et al., 2020; M. Zhang et al., 2021), especially in the tide-dominated estuaries, where intertidal flats were commonly wide (Syvitski et al., 2009; X. Wang et al., 2021). As a result, the tide-dominated estuaries worldwide have experienced a massive morphological shrinking, and few still preserve the original wide tidal flat, leading to riparian habitat loss and flood protection failure (Dai et al., 2016; Wei et al., 2017). In China, the magnitude of reclamation increased dramatically with the explosive growth of the economy, which posed a big challenge for the sustainable development of tide-dominated estuaries (W. Wang et al., 2014). Recently, following

the implementation of the Chinese new coastal protection policies (Sheng et al., 2022; X. Wang et al., 2021), evaluating the impact of anthropogenic reclamation works and estimating the tide-dominated estuary's evolutionary fate are urgently necessary for their proper water resources management.

Ideal model studies showed that the morphology of tide-dominated estuaries was inherently more stable than wave- or fluvial-dominated estuaries because tidal motions are more predictable, acting to stabilize the system (Dalrymple & Choi, 2007; Fagherazzi, 2008; Hoitink et al., 2017). This is particularly true for North Branch (NB), the northern first-order distributary of Yangtze Estuary (see Figure 1), where the system is large and the tide is strong (Leonardi et al., 2021). In order to explain the channel re-adjustment after anthropogenic disturbance, several process-based morphodynamic models for the tidal estuaries and coastal areas have been developed (Luan et al., 2016; van der Wegen et al., 2008; Zhou et al., 2018). G. D. Gao et al. (2014), Hoitink et al. (2003), and Zhou et al. (2018) tried to unveil the mechanism of the tide-dominated system with tidal asymmetry theory for the induced channel re-adjustment after local disturbances, for example, dredging the channel tends to cause deposition by increased flood tidal asymmetry, while reclaiming the intertidal areas leads to subtidal erosion by reduced flood tidal asymmetry. However, few researchers have explored the mechanism of nonlinear effect that drives the system adjustment between fast development and equilibrium states, mostly focusing on the effects of negative feedback process (van der Wegen et al., 2008; Y. Wang et al., 2013; Zhou et al., 2018) or positive feedback process (X. Zhang, Fagherazzi, et al., 2018), especially for a large system like NB, where dredging was almost not existed, and extensive reclamations were performed for land demand (Dai et al., 2016) and mitigating saltwater intrusion (Kuang et al., 2021; E. Zhang, Townend, et al., 2019) purposes. Understanding the feedback mechanism of such dynamic evolution is crucial for estuary restoration and maintenance works after substantial anthropogenic disturbances.

Changjiang River, stretching for approximately 6,300 km from the Tibetan Plateau to the East China Sea, is the largest river in China and drains a catchment of approximately 1.8 million km² (Figure 1a). Estuary studies typically focus on the reach downstream of Datong (Figure 1a), where there is a hydrological station that is approximately at the upstream limit of tidal propagation during the dry season (M. Zhang et al., 2016). Tidal effects become significant downstream of the giant bend approximately 250 km from the mouth and dominant over the last 150–200 km (M. Zhang et al., 2016). Downstream of Xuliujing (Figure 1b), the estuary bifurcates into the South Branch (SB) and NB, which is mainly tide dominant. Further downstream, the SB divides into the North Channel and South Channel. Finally, the North Passage and South Passage form the main channels through the large subaqueous delta at the bar area of the estuary, where the mouth is about 90 km wide (Figure 1b). This well-defined branching and delta system was resulted from a long-term, uninterrupted prograding processes (Dai et al., 2014; S. Gao, 2013). The historical movement of coastlines and island attachment frequently occurred during the past 3,000 years (J. Chen et al., 1979). As is shown (Figure 1b), the Changjiang River mouth was wide open in the year 1000 B.C., similar to the present Hangzhou Bay of China (J. Chen et al., 1979); the river mouth was moved downstream to around Yangzhou and Zhenjiang and further to Jiangyin approximately in the 8th century and 17th century, respectively (Figure 1b). Now, the estuarine mouth opens around Shanghai at the Qidong cape and Nanhui spit (Figure 1b).

Recent studies of NB have explored the saline water intrusions (Kuang et al., 2021; E. Zhang, Townend, et al., 2019) and the sediment dynamics (Dai et al., 2016; Guo et al., 2022; Li et al., 2015) of the tide-dominated system, and the influence of large-scale engineering works implemented at upstream (Yu et al., 2014) and in the SB (Luan et al., 2016). However, little is known about the possible future evolution trend and equilibrium adjustment mechanism of the tide-dominated system under intensive reclamations. Moreover, there is a continuous international debate about the impact of many dams installed at upstream in the Changjiang River (X. Chen et al., 2008; Luan et al., 2016) and the response of the subaqueous delta to the decreased sediment supplies (Li et al., 2015; Nienhuis et al., 2020). Long-term sediment flux change from the catchment was proved to have a significant influence on the downstream morphodynamics (Dai et al., 2018; Mei et al., 2021), and the overall subaqueous delta had suffered from erosion due to the drastic decrease of sediment load (Luan et al., 2016). However, Leonardi et al. (2021) pointed out that the Suspended Sediment Concentration (SSC) outside of the Yangtze Estuary was crucial for the development of NB because sediment can be compensated from the sea due to the tide-dominated flows. In addition, Y. Wang et al. (2013) showed that local-scale morphology disturbance, such as reclamation, was more influential for channel development than the upstream environment changes (Y. Wang et al., 2013). To clarify this point, Dai et al. (2016) tried to link the infilling of NB to anthropogenic reclamation despite the decreased sediment supply from upstream (Dai et al., 2016). A similar process demonstrated in
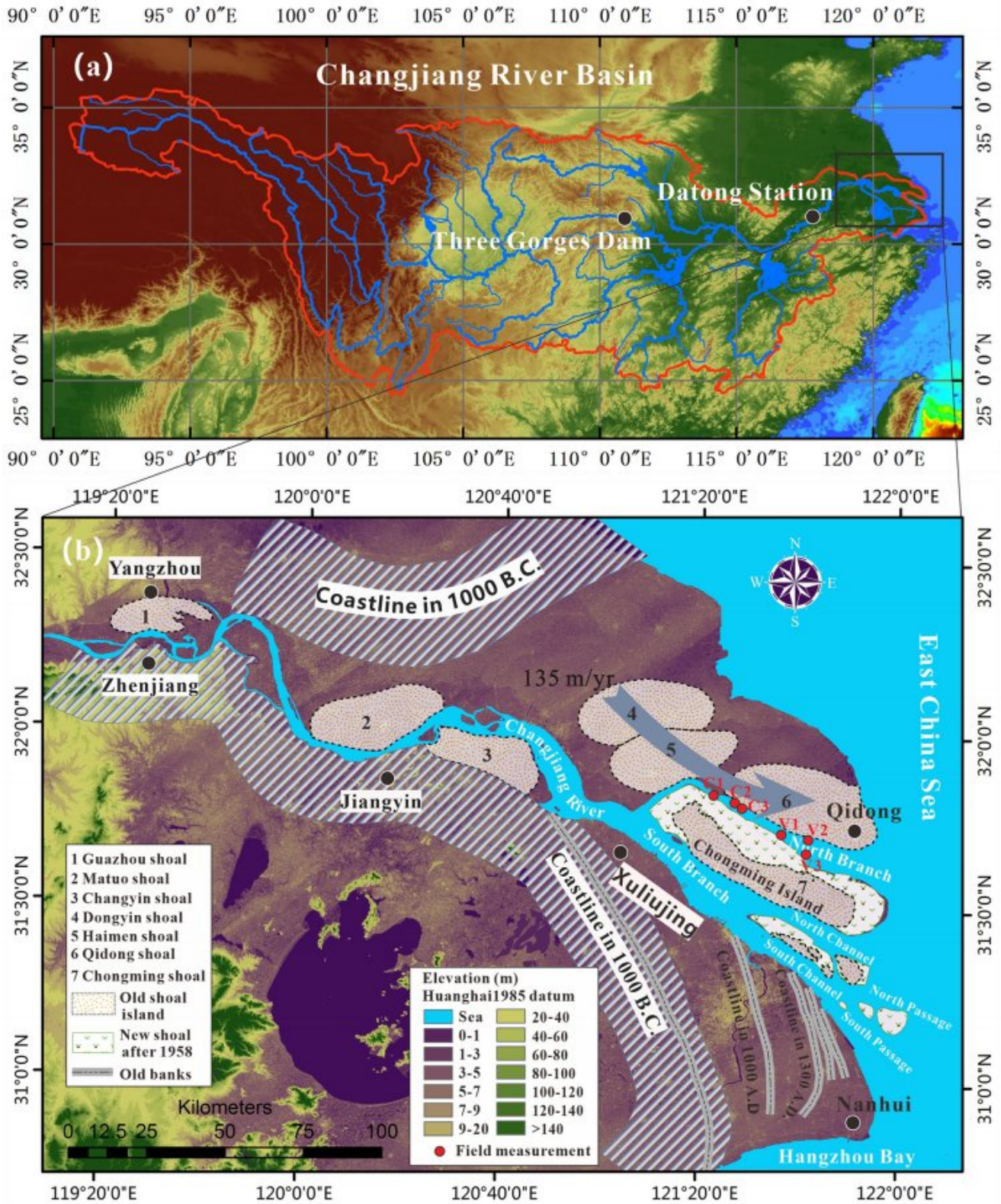
Figure 1. Sketch map of the research area. (a) The location of the Yangtze Estuary and Changjiang River Basin in China, and (b) the branching and movement of the historical Yangtze Estuary and the shoal islands.

Table 1
Monthly Averaged Water Discharge (WD) and Sediment Discharge (SD) During Three Typical Historical Periods (Luan et al., 2017), That Is, 1958–1984, 1984–1997, and 2001–2020

WD (10^3 m^3/s)												
SD (ton/s)	January	February	March	April	May	June	July	August	September	October	November	December
1958–1984	10	10.5	14.5	23	36	40.1	48.5	40.1	36.5	32	22.5	14
	1.3	1.3	2.8	7.2	17.0	19.0	38.0	32.5	29.0	19.5	8.0	3.5
1984–1997	11.5	13.5	16.5	25.5	30.5	38.5	53	44	38	30.1	21	14.8
	1.2	1.3	3.0	5.0	7.0	14.0	30.0	27.0	24.0	14.0	5.5	2.2
2001–2020	12.5	14	19	22.5	33	39.5	46	43	39	26.5	19.5	14.8
	1.4	1.5	3.1	4.2	6.0	7.3	11.5	12.5	10.0	4.5	3.5	2.0

Hangzhou Bay, bordering the Yangtze Estuary, proved that anthropogenic reclamation overwhelmed the change of sediment supply on local morphological adjustment (Xie et al., 2017). The evaluation of morphology disturbance under reclamations and sediment-starving conditions for the tide-dominated estuary attracts great concerns of the influence it may have on the evolutionary fate of NB, which remains essentially unstudied.

In this paper, we focused on the NB, the tide-dominated distributary of Yangtze Estuary, to (a) explore the impact of anthropogenic disturbance on channel re-adjustment over the last 50 years and, (b) model the effect of hydrodynamic feedbacks on morphology evolution over the next 100 years, based on a series of historical maritime charts and a coupled hydro-morphodynamic model. The research aims are to (a) explore the morphology evolution pattern of NB; (b) examine the morphology equilibrium and adjustment mechanism of NB under intensive anthropogenic interventions; (c) predict the future NB evolution under the implementation of coastal preservation policies. The results presented herein may be relevant to other tide-dominated estuaries subject to large-scale human interventions, such as reclamation works at the local scale and decreased sediment supply from upstream damming.

2. Material and Methods

2.1. Data Sources

In this research, nine navigation charts covering NB and the surrounding area in 1958, 1978, 1984, 1991, 1998, 2001, 2007, 2010, and 2020 were collected from the Maritime Survey Bureau of Shanghai, Ministry of Communications of China. The scale of the maps is 1:50,000 in the NB and 1:100,000 in the estuary bar area. The vertical error of the measurement was declared to be 0.1 m (Dai et al., 2016). The 2008 navigation charts, covering the lower reach of Yangtze River from Datong to Xuliujing, the 2007 maritime chart, covering SB and the bar area as well as GEBCO (General Bathymetric Chart of the Oceans) database, covering the continental shelf area, were collected. Historical coastline positions were set at seawalls and dikes obtained directly from observations of historical navigation charts and archived satellite images (http://glovis.usgs.gov/). They were all merged and expressed relative to the Huanghai 1985 national elevation datum and converted to UTM-51 Geodetic Coordinate. The reclamation area and coastline movement identified at seawalls were then obtained by spatial-temporal analysis of the consecutive coastline changes performed in ArcGIS10.1.

The data on monthly water and Sediment Discharge (SD) collected at the Datong station during 1958–2020 were obtained from the Changjiang Water Resources Commission (http://www.cjh.com.cn/). Statistics show the monthly averaged Water Discharge (WD) and SD in the wet and dry seasons during three typical historical periods, that is, 1958–1984, 1984–1997, and 2001–2020 (Table 1). They were used to define the long-term river boundary conditions. Tidal constituents driving the sea boundary were generated by TPXO (TOPEX/POSEIDON global tidal model data set) with harmonic compositing of eight primaries, two long periods, and three nonlinear constituents (M. Zhang, Townend, et al., 2019). The absolute sea-level rise reconstruction in the past 50 years and estimation over the next 100 years were generated based on previous literature (Church et al., 2004; M. Zhang, Townend, et al., 2019), which collectively suggested an approximately 1.9 times faster rate at the NB than the global mean value. Relative to the 1958 sea level, water depth increases of 0, 0.095, 0.124, 0.157, 0.19, 0.204, 0.233, 0.247, and 0.251 m were applied to the collected nine sets of historical bathymetries. The
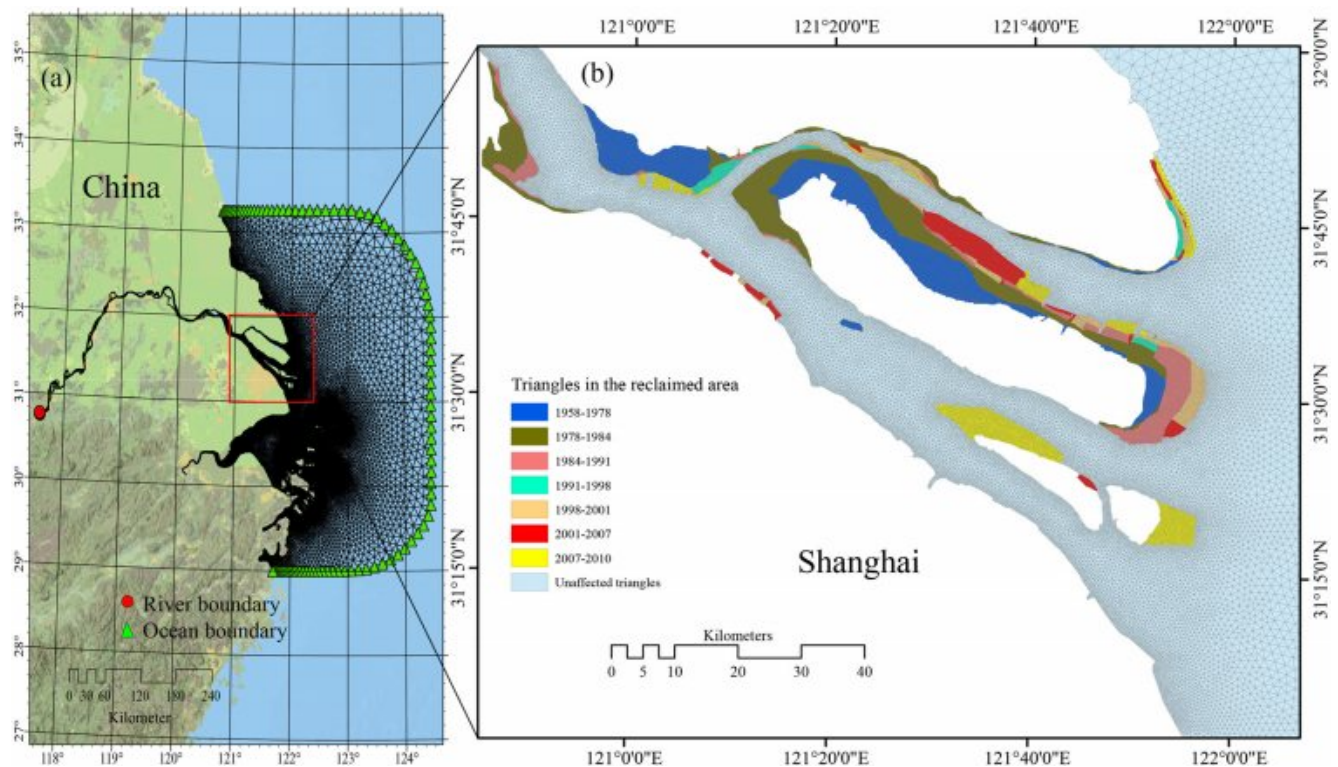
Figure 2. Maps of irregular triangular meshes. (a) The large-scale modeling domain covering Yangtze Estuary, Hangzhou Bay, and the continental shelf area, and (b) an enlarged view showing the change of triangular meshes in North Branch that were added, removed, or moved following reclamations during the examined periods.

sea-level variations in NB were generated automatically by the hydrodynamics model because the effects of river-tide-morphology interactions were built-in programs solved by the numerical model (Du et al., 2018). Monthly averaged salinity distribution digitized from Kuang et al. (2021) and E. Zhang, Gao, et al. (2019) was prescribed along NB, which was only used for a simple flocculation model.

2.2. Hydrodynamics Modeling and Validation

A two-dimensional numerical model of TELEMAC-2D was constructed to reproduce historical hydrodynamic flows in NB (Hervouet, 2007). First, model setup and model validation of the hydrodynamic system were performed using one of the time intervals of the available bathymetry (i.e., 2007) bounded with 2005 coastline interpreted from satellite TM image, then the validated model was rerun with consistent forcing for all other available bathymetries (e.g., 1958, 1978, 1984, 1991, 1998, 2001, and 2010). The model domain, extending from Datong station at upstream to the continental shelf in the East China Sea, was configured with irregular triangular meshes with varying lengths of over 10,000 m at offshore to 200–300 m at nearshore, resulting in approximately 45,000 meshes and 45% of the elements located within the study area (Figure 2). In order to produce a precise comparison, the domain of triangles unaffected by coastline changes was kept constant, that is, only the triangles falling in the reclaimed areas were added or removed following the sequence of reclamations (Figure 2b). The available bathymetries for historical variation study only covered the NB. Therefore, the rest meshes in the domain were kept unchanged. The seaward boundary was determined with changing ocean conditions provided by TPXO, taking account of sea-level rise and the variations in the meso-tidal range; similarly, the landward boundary was defined with changing river conditions over the study period, taking account of signals representing the seasonal and inter-annual variations in water and SDs (Table 1). For detailed descriptions of hydrodynamics parameter setups and configurations of the Yangtze Estuary model, readers can refer to our previous publications (e.g., M. Zhang, Fagherazzi, et al., 2018; M. Zhang, Townend, et al., 2019, and M. Zhang et al., 2021).

In order to perform model calibration and validation of the hydro-morphodynamic simulation, three cruise surveys were carried out purposely in the NB during 17–18 July 2005 for calibration (C_1, C_2, and C_3) and 19–20 July
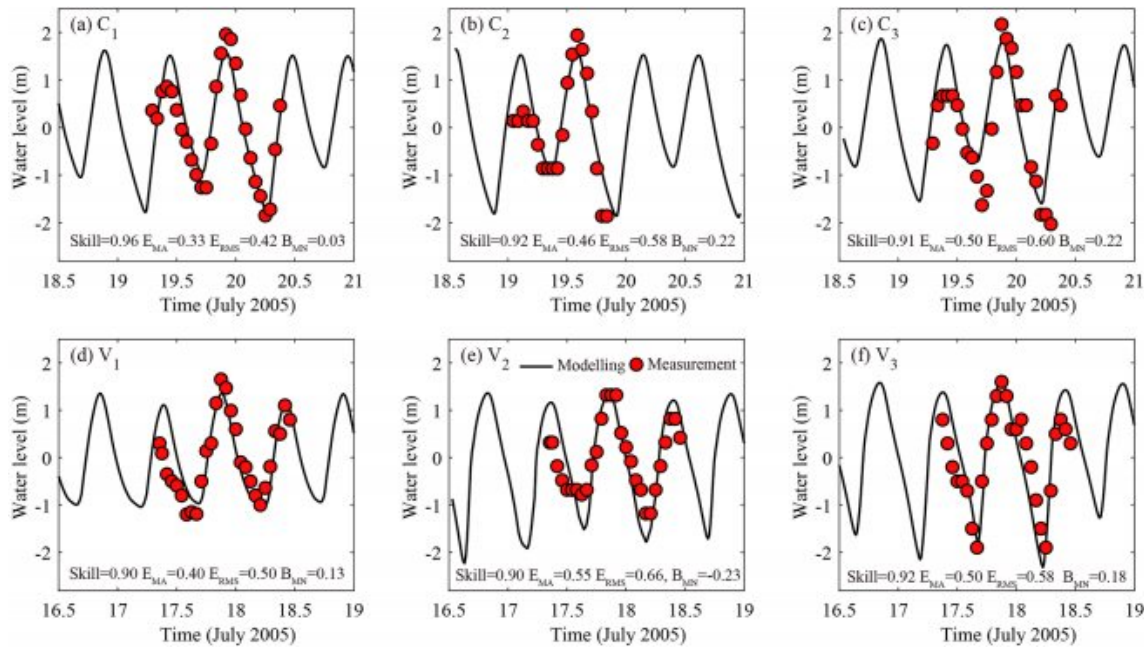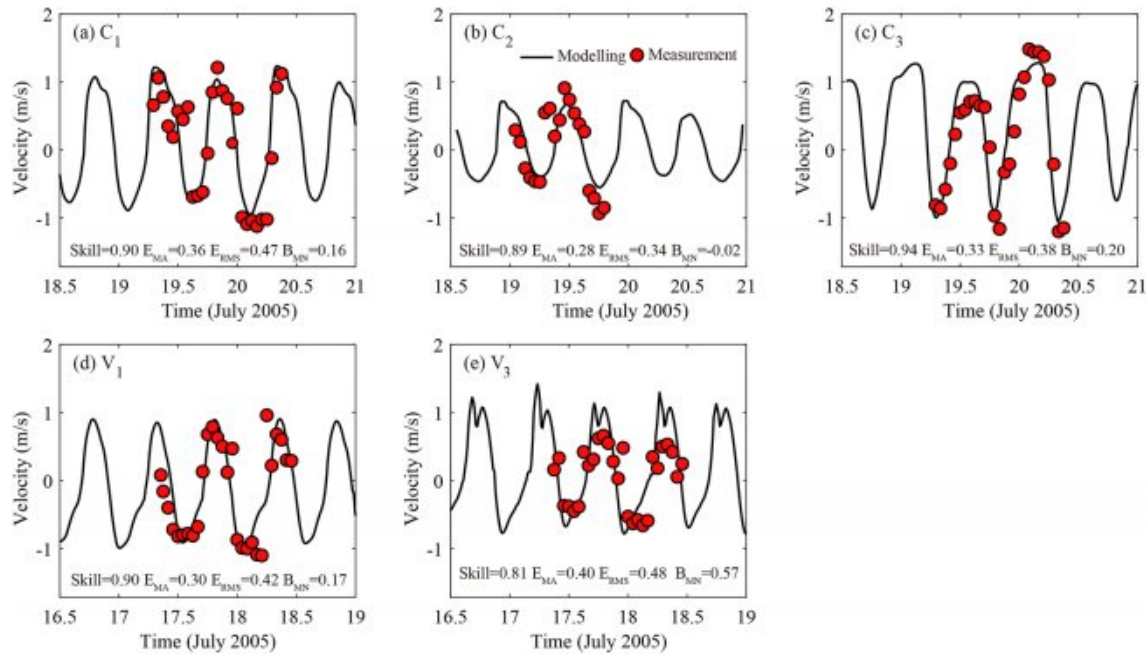
Figure 3. Hydrodynamics modeling calibration (a–c) and validation (d–f) for the observed free surface, with statistical evaluation criteria of skill value, mean-absolute error (E_{MA}), root-mean-squared error (E_{RMS}), and mean-normalized bias (B_{MN}). Station C_2 contains only 20 hr due to boat and instrument grounding.

2005 for validation (V_1, V_2, and V_3), respectively. They were specifically designed to measure the nature of tidal and sediment dynamics during flood and ebb periods in the high river discharge season. A total of six measuring locations were placed along the NB, that is, C_1, C_2, C_3, and V_1, V_2, V_3 (Figure 1b). Anchored measurements of 27 hr (covering two complete tidal cycles, except C_2 containing only 20 hr due to boat and instrument grounding) by the three boats were first taken place synchronously at C_1, C_2, and C_3. They were then moved together to V_1, V_2, and V_3 by spending another 28 hr for measurements. Acoustic doppler current profiler (SonTek-500), direct-read current meters (SLC9-2), and OBS-3A (5 MHz) were used to measure the flow direction, flow velocity, and turbidity, respectively, at water depths of 0H, 0.2H, 0.4H, 0.6H, 0.8H, and H (0.2 m above the seabed, here H represents the water depth) every 1 hr. Water samples collected at each water depth were filtered in the laboratory to obtain grain size and density (SSC). The comparison between observed and predicted free surfaces and flow velocities at the sampling locations were shown explicitly in Figures 3 and 4, with the quantified evaluation of the agreement using four criteria: mean-absolute error (E_{MA}), root-mean-squared error (E_{RMS}), mean-normalized bias (B_{MN}), and skill value (M. Zhang et al., 2021). Overall, the model reasonably reproduced the water level and velocity of the tides, and the model average skill value reached up to 0.92 for free surfaces and 0.89 for flow velocities, indicating the good performance of the hydrodynamic simulation. The maximum error of the flow velocities occurred at the V_3 station, with the E_{MA}, E_{RMS}, and B_{MN} values being 0.50, 0.48, and 0.57 m/s, respectively; The maximum error of the free surfaces occurred at the C_3 and V_2 stations, with the E_{MA}, E_{RMS}, and B_{MN} values being 0.50 and 0.55 m, 0.6 and 0.66 m, and 0.22 and −0.23 m (negative indicating under-prediction), respectively, possibly for the reasons of local disturbance and inconsistency in years between the used bathymetry and the field measurements.

2.3. Morphodynamic Modeling, Sensitivity Analysis, and Validation

The future evolution of NB morphology was modeled with MIKE21FM, a mud transport module of the MIKE software by DHI (www.dhigroup.com), to reproduce the sediment transport process. The morphodynamic modeling was set up starting from the 2010 bathymetry and forced with astronomical tide predicted until 2100 without anthropogenic disturbance. The distribution of suspended sediments was defined using 530 sediment samples collected at six locations by the three boats during July 2005 (Figure 1b). The average mean grain size (D_{50}) was measured to be approximately 42 μm with coarser sediments (∼58 μm) observed in the inner NB (C_1, C_2, and C_3) and finer sediments (∼31 μm) observed in the outer NB (V_1, V_2, and V_3). The resulting distribution

Figure 4. Hydrodynamics modeling calibration (a–c) and validation (d–e) for the observed flow velocity, with statistical evaluation criteria of skill value, mean-absolute error (E_{MA}), root-mean-squared error (E_{RMS}), and mean-normalized bias (B_{MN}). Flow velocities observed at station V_2 were unavailable due to instrument failure.

of suspended sediment is similar to those reported by Li et al. (2015) and X. Zhang, Fagherazzi, et al. (2018). Because of the complexity and high spatial variability of the sediment composition (Li et al., 2015; X. Zhang, Fagherazzi, et al., 2018), implementing the model with spatially variable grain size distribution would be difficult and computationally expensive. Therefore, the modeled sedimentation process in the water column was configured with purely cohesive sediments with a diameter of less than 60 μm (Luan et al., 2017). Specifically, we set the suspended sediment with two fractions, that is, a mixing of coarse cohesive sediment of $D_{50} = 58$ μm and fine cohesive sediment of $D_{50} = 31$ μm, representative of the range of sediments measured in the NB (see Table 2). The sediment concentration at the ocean boundary was set to zero due to the deep ocean being far away from NB, while the river boundary was configured with schematized suspended SD (see Table 1), representing the seasonal and inter-annual variations at the Datong station (Luan et al., 2017). The settling velocities of the two fractions of suspended sediments, estimated using Stokes law, were set to 0.0002 and 0.0004 m/s, respectively, while the real sediment settling velocity was calculated dependent on the grain size with flocculation considered

Table 2
Hydro-Morphodynamic Parameters and Configurations Used in North Branch Modeling Study

Parameter	Symbol	Value	Unit	Source
Uniform friction coefficient	M	45	$m^{1/3}/s$	Mi et al. (2022)
Eddy viscosity	C_S	0.28	m^2/s	Smagorinsky (1963)
Dry sediment density	ρ_d	550	kg/m^3	Luan et al. (2017)
Acceleration factor	AF	200	–	–
Cohesive sediment diameter (fine ∼ coarse)	D_{50}	31–58	μm	Measured
Sediment settling velocity (fine ∼ coarse)	W_s	0.0002–0.0004	m/s	Sternberg et al. (1999)
Critical shear stress for sediment deposition (fine ∼ coarse)	τ_{cd}	0.03–0.06	N/m^2	X. Zhang, Fagherazzi, et al. (2018)
Critical shear stress for sediment erosion (fine ∼ coarse)	τ_{ce}	0.6–0.12	N/m^2	X. Zhang, Fagherazzi, et al. (2018)
Maximum floc settling velocity	W_{floc}	0.005	m/s	Luan et al. (2017)

after calibrating the model against the spatial distribution of the depth-averaged SSC (Sternberg et al., 1999). A simplified flocculation model that relates the floc settling velocity to the water salinity was applied, with the maximum floc settling velocity set to 0.005 m/s (Luan et al., 2017). Deposition occurs where the bed shear stress of driving force (τ_b) was smaller than the critical shear stress of deposition (τ_{cd}), which were set to constant values of 0.03 N/m² for fine sediment and 0.06 N/m² for coarse sediment after calibration (Table 2). The deposition for the ith mud fraction in the water column is described as:

$$D^i = W_s^i c_b^i P_D^i,$$

(1)

$$P_D^i = \max\left(0, \min\left(1, 1 - \frac{\tau_b}{\tau_{cd}^i}\right)\right),$$

(2)

where P_D^i is probability ramp function of deposition, W_s^i is the settling velocity (m/s), and c_b^i is the near bed sediment concentration (kg/m³), τ_b and τ_{cd}^i are real-time bottom shear stress and critical shear stress (N/m²) for deposition, respectively.

The modeled sedimentation process in the bed was configured with bed parameters, including dry density, erosion intensity, and bed roughness (X. Zhang, Fagherazzi, et al., 2018). We assumed the bed property as densely consolidated hard mud with a dry sediment density of 550 kg/m³ (Luan et al., 2017). The criteria for erosion were defined as bed shear stress of imposed driving force (τ_b) exceeding the critical shear stress for erosion (τ_{ce}), which was set to a combination of constant values of 0.12 and 0.6 N/m² of the applied two fractions to account for the variety of states (consolidation, water content, etc.) in which muddy sediments presented in NB (X. Zhang, Fagherazzi, et al., 2018). For the densely consolidated bed, the mass of each fraction (i) of the bed sediment was updated every time step in the mesh grid following the expression given by Partheniades (1965):

$$m_i^{new} = m_i^{old} + (D - E)\Delta t,$$

(3)

$$E = E_0 P_E,$$

(4)

$$P_E = \max\left(1, \frac{\tau_b}{\tau_{ce}^i}\right),$$

(5)

where m is sediment mass (kg/m²), D is possible deposition (kg/m²/s), E is possible erosion (kg/m²/s), P_E is probability ramp function of erosion, Δt is simulation time step (s), and E_0 is the erosion coefficient.

In shallow estuarine and coastal areas, it is necessary to consider the feedbacks of morphological change on the hydrodynamics, especially for the long-term morphological evolution simulations (van der Wegen et al., 2008). Here, the long-term morphology updating was accelerated by multiplying an accelerating factor (*AF*) with the net sedimentation for every time step (set to 30 s) in bathymetry modeling. This ensures a stable bed evolution to accelerate the morphology change, meanwhile it will not destabilize the hydrodynamics simulation. The adopted *AF* equation is:

$$Z^{n+1} = Z^n + \Delta Z^n \times AF,$$

(6)

where Z^n is bathymetry level at present timestep (m), Z^{n+1} is bathymetry level at the next time step (m), ΔZ is sedimentation change at present timestep (m), *AF* is a dimensionless accelerate factor defined as an integer.

For a specific location, the periods of peak flow and slack water are crucial for the erosion and deposition of sediments (Dronkers, 1986). We tested varied critical shear stress for deposition τ_{cd} (0.03–0.06 N/m²) and erosion τ_{ce} (0.12–0.6 N/m²), representing the range of relative fraction of fine (31 μm) and coarse (58 μm) sediments that matched the measured mean grain size in NB. We obtained a similar morphology evolution pattern of NB but with a faster evolution speed for coarse sediment and slower evolution speed for fine sediment, which were offset by applying an appropriate accelerate factor *AF* (approximately 125–300) to fulfill the morphology calibration and validation requirements (Figure 5). Generally, higher *AF* values lead to larger spatial phase shifts and a more diffused character of morphology pattern (van der Wegen et al., 2008), however there exists no robust and objective method for determining the highest *AF* for a given simulation (Luan et al., 2016). The sensitivity test indicated that an *AF* of 200 was appropriate for the current century-scale simulation for a composition of 50% fine sediment and 50% coarse sediment (Figure 5). Therefore, the first 1.5 days, representing 1 year by considering
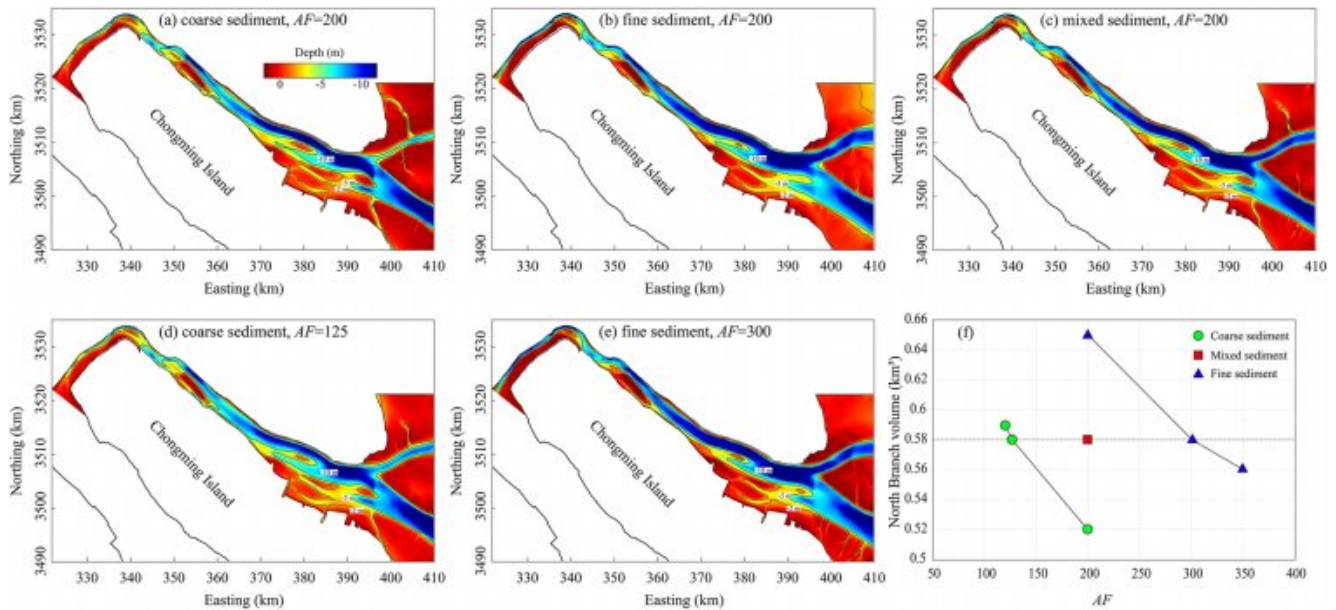
Figure 5. Sensitivity test of the morphodynamic evolution with the applied modeling configurations for (a) coarse sediment, (b) fine sediment, and (c) combining 50% fine sediment and 50% coarse sediment with the same accelerating factor (AF) value of 200, (d, e) with a varying AF value from 125 to 300, and (f) the statistics comparison of North Branch volume for the applied AF value and sediment compositions.

the applied AF, were treated as the warm-up period, and the morphodynamic model ran for the next 160 days, representing 90 years, to the year 2100.

The selected periods from 1990 to 1998 and 2010 to 2020 with the least human reclamation disturbances were used for morphodynamic model calibration and validation (Figure 6). Starting from 1990 bathymetry, the modeled 1998 bathymetry showed good comparisons with the measured 1998 bathymetry, that is, in the lower reach, the shoals above −5 m contour accreted and channels of −10 contour deepened; in the middle reach, the shallow shoals moved downstream and enlonged the −5 m contour by more than 5 km to block the deep channel; in the upper reach, the meandering channels showed continuous development and deposited on the southern bank of the turning. For the model validation of 2020 bathymetry, starting from 2010 bathymetry, 10 years of morphodynamic change was generated. However, only the comparison of the deep channel was performed because the field measurement in the shoals and intertidal areas were unavailable. Overall, the morphodynamic model captured the main evolution pattern of NB development, which shows good statistical skill values of 0.65 for calibration and 0.73 for validation, with relatively large difference at the transition area between intertidal and subtidal zones (Figures 6d and 6h).

2.4. Scenario Simulation and Analytical Metrics

All model configurations and boundary conditions implemented in the scenario simulations were held constant, for example, for the historical investigations, only the bathymetries and coastlines were manually updated, while for the future morphology predictions, the bathymetry evolution starting from 2010 were automatically shaped by the hydrodynamic forcing. For all simulations, the model output, comprising water level and flow velocity, was then processed to derive a number of metrics indicating estuary stability. For this purpose, a series of cross-sections (N1–N16) were defined at approximately 5.5 km intervals along the axis of NB (Figure 7a–7i). At each cross-section, the water levels and velocities normal to the cross-section were extracted as section average, and the variation of cross-section area relative to the dynamic water surface (DWS), that is, the high and low water surfaces varying spatially along the estuary, was computed. For each reach between two adjacent cross-sections, volumes and surface areas were also obtained. These were calculated using a series of horizontal planes at intervals through the vertical to define a hypsometry and relative to the high and low water surfaces to track changes in subtidal and intertidal volumes. Notably, the DWS of high and low water levels were constructed from water levels at different times during the tidal cycle because the time of high and low water varied along the
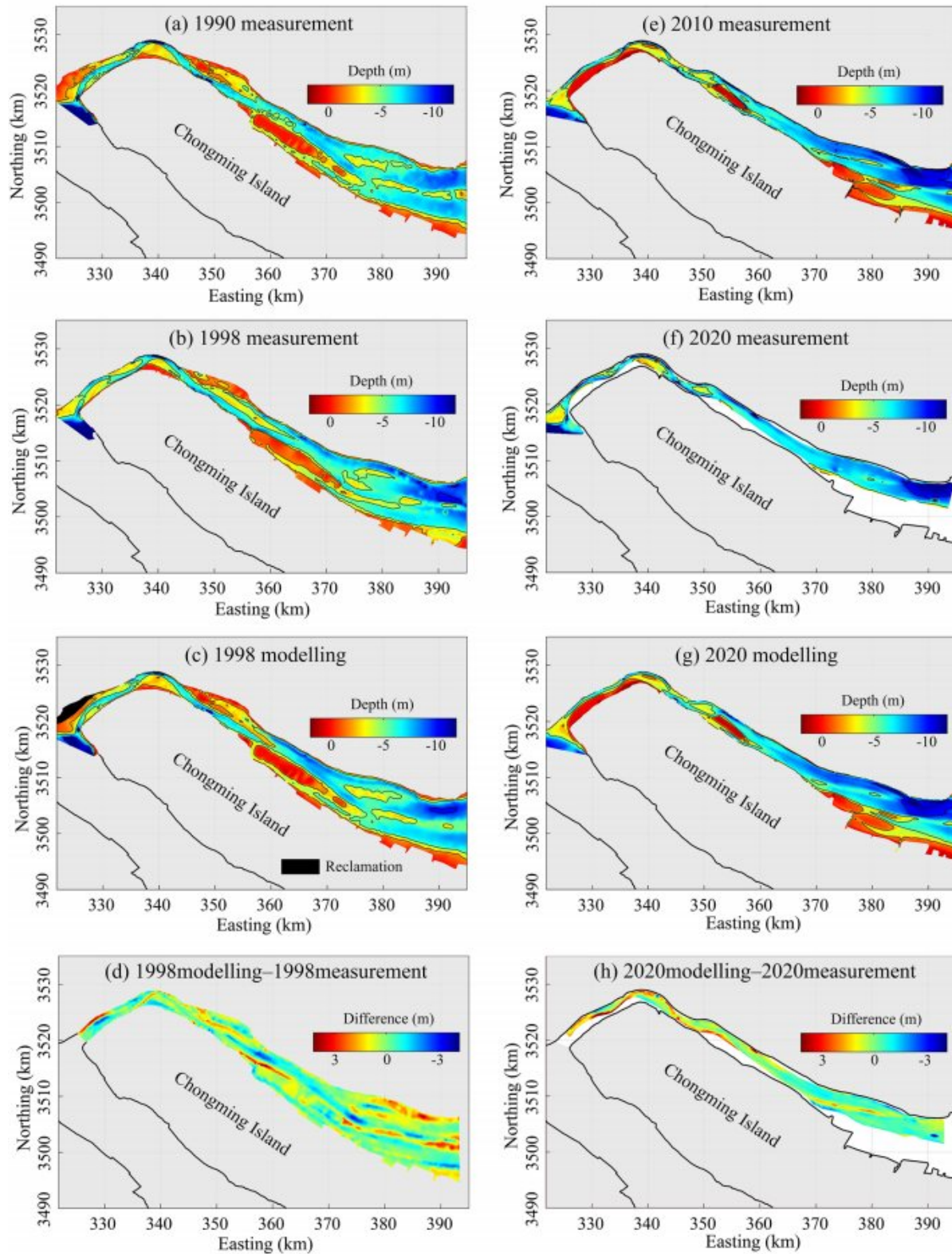
Figure 6. Morphodynamic modeling (a–c) calibration from 1990 to 1998 and (e–g) validation from 2010 to 2020 for the bathymetries with minor reclamation disturbance. Subplots (d, h) show the difference between the modeled bathymetry and measured bathymetry.
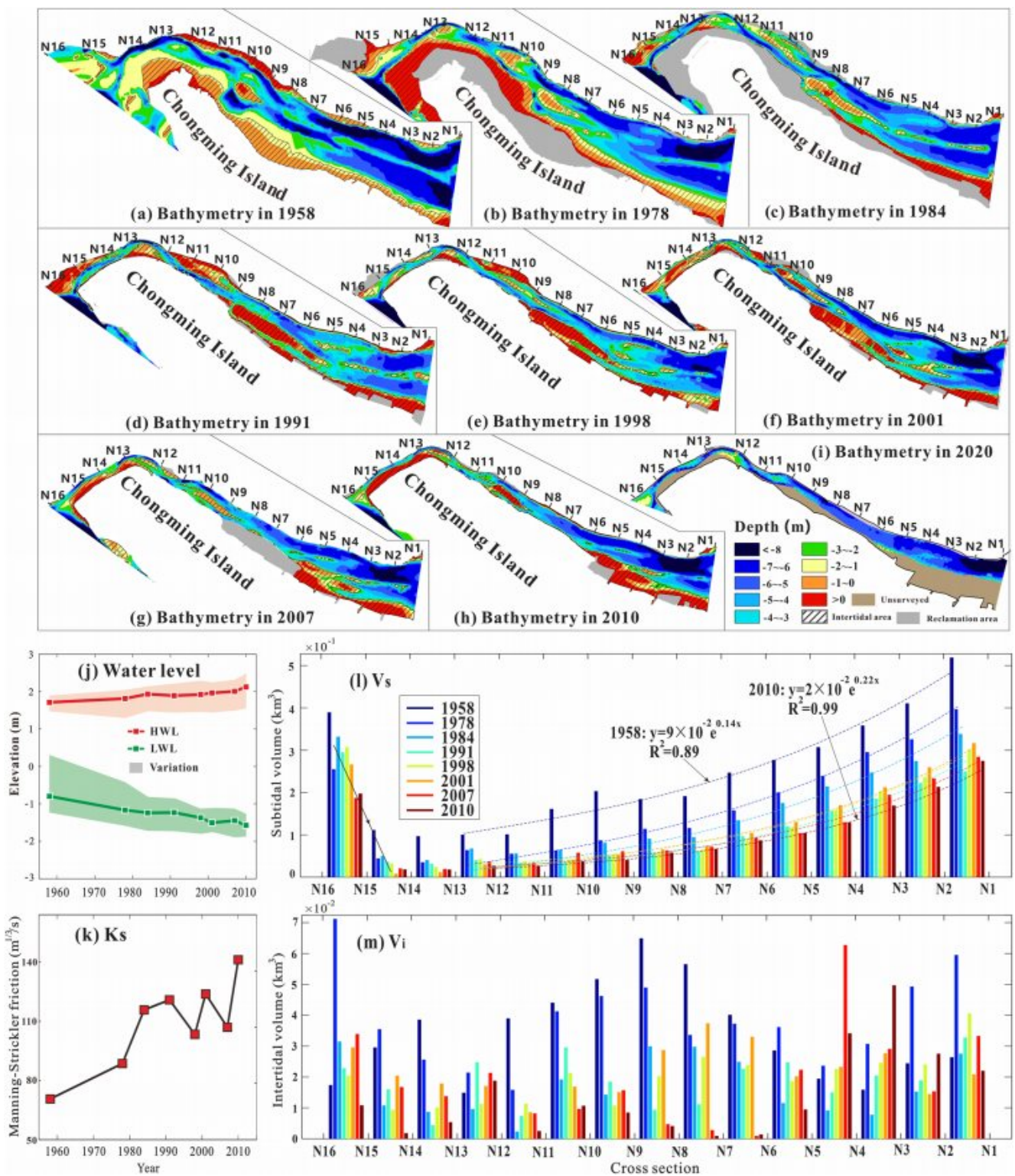
Figure 7. The historical change of North Branch (NB) bathymetry and the induced hydrodynamic parameter variation. (a–i) Measured NB water depth and the variation in the intertidal area from 1958 to 2020. (j) NB-averaged high-water level and low-water level change from 1958 to 2010. (k) NB averaged friction coefficient (K_s) change from 1958 to 2010. (l, m) Sectional subtidal (V_s) and intertidal (V_i) volume change along NB from 1958 to 2010. The bathymetry of 2020 is only available in the navigation channel.

estuary (Townend, 2012). The DWS of high and low water levels were considered because reclamations usually take place at the intertidal area, and under a rising sea level, bathymetries above high-water level (HWL) need to be considered, as the accommodation space that the estuary "moves into" can influence the hydrodynamic responses (Townend, 2012). Here, the selected metrics used for analysis are described as follows.

1. Metrics of hydrology, for example, DWS of HWL and low-water level (LWL) is defined as the local highest and lowest tidal level, which vary spatially along the estuary; the lower margin of the intertidal area is defined at the water boundary of LWL; tidal amplitude (η) is defined as the tidal range between HWL and LWL; tidal duration asymmetry (TDA) is defined with the indicators of magnitude difference, denoted by A_{M_4/M_2} and phase difference, denoted by $2\varphi_{M_2} - \varphi_{M_4}$, where flood and ebb dominant systems have relative sea surface phases of 0°–180° and 180°–360°, respectively, and for a fixed relative phase, the larger the A_{M_4/M_2}, the greater the magnitude of distortion and the more strongly flood or ebb dominant the system becomes (Friedrichs et al., 1990); peak current asymmetry and slack water asymmetry (SWA) are calculated using the skewness method following Guo et al. (2018); the Manning-Strickler friction factor Ks is estimated using the dimensional damping equation and calibrated parameters of storage width ratio provided by Cai et al. (2016); tidal prism (TP) is defined as the flood tidal discharge volume corrected for the influence of the river discharge (M. Zhang et al., 2016).

2. Metrics of geometry, for example, the channel volume (V_t) is defined between the bathymetry and the DWS of HWL and LWL, in which the subtidal volume (V_s) is defined between the LWL and bathymetry, and the intertidal volume (V_i) is defined between the HWL and intertidal bathymetry. Hence, the total channel volume is defined as $V_t = V_s + V_i$, where the V_t reduction due to human activity can be primarily attributed to land reclamation (R), which is defined as the volume change between the reduced intertidal bathymetry and HWL, while the V_t change due to nature force is erosion (E) or accretion (A), which is defined as the difference between the remaining channel volume after reclamation and the measured channel volume in the next period (before reclamation).

3. Metrics of energy, for example, the metrics of energy flux, energy dissipation, minimum entropy production, and maximum work, were obtained. The energy head (J/m²) is defined as the time-dependent energy per unit width (M. Zhang et al., 2016). The energy flux (J/s) was obtained by integrating the energy head over the transverse section, and when integrated over a tidal cycle gives the cycle energy (J) passing through the section. The energy dissipation ΔE (J) is defined as the total energy flux (river and tide) entering and exiting the system (M. Zhang, Townend, et al., 2019), and when dividing by the total energy input leading to the energy dissipation ratio γ, that is, the energy contribution to the work done globally (M. Zhang et al., 2016). The adopted equations are defined as:

$$F = uBe, \tag{7}$$

$$E = \int F\,dt, \tag{8}$$

$$\Delta E = E_{\text{enter}} - E_{\text{exit}}, \tag{9}$$

$$\gamma = \frac{\Delta E}{E_{\text{enter}}}, \tag{10}$$

where u is the cross-sectionally averaged flow velocity (m/s) with positive pointing to the upstream direction and negative pointing to the downstream direction, B is the channel width (m), e is the energy head per unit width (J/m²), F is the instant energy flux (J/s), E, E_{enter}, and E_{exit} are the energy flux over a tidal cycle along the estuary axis, at the entrance, and at the exit of the system, respectively.

Following Townend and Dun (2000) and van der Wegen et al. (2008), the entropy production $d\varphi$ for bi-directional discharge estuaries can be expressed by evaluating the total energy flux over a tidal cycle. For the energy contribution to the work done locally, it is suggested that the entropy production per unit volume near equilibrium will tend to evolve to a minimum compatible with the boundary conditions imposed on the

system when the total energy flux follows an exponential distribution (Townend & Dun, 2000). The adopted equations are defined as:

$$d\varphi = \frac{1}{\int |F| dt} \frac{d(\int |F| dt)}{dx}, \tag{11}$$

$$\int |F| dt = D \exp(Cx), \tag{12}$$

where $d\varphi$ is the entropy production (per meter), C and D are constants, x is the distance from the estuary mouth. Finally, we compared the total energy flux to the suggested theoretical "most probable" distribution directly following Townend and Dun (2000).

3. Results

3.1. Geomorphology Evolution of NB

Under anthropogenic interventions of embankments and reclamations, the intertidal space of NB gradually vanished, and the channel became more constrained. Spatially, the intertidal area of the low-slope tidal flat was 2–5 km wide at the beginning when the margin of LWL meandered between the broad areas of 0 to −2 m contours in 1958 (Figure 7a). However, after massive reclamations of 550 km² between 1958 and 1984, the intertidal area was reduced dramatically to only 103 km², and the margin of LWL was pushed seaward to a narrow zone almost consistent with the −2 m contour (Figure 7d–7i). The subtidal volume (V_s), on the other hand, showed a clear double channel pattern in the first 30 years (1958–1984) when the average depth was −5.5 m. Following reclamations, the southern channel then gradually vanished during 1991–2001, replaced with fragmented intertidal-cut shallow channels, and finally turned into intertidal space entirely in the last 10 years (2001–2010). The northern channel showed a slightly narrower and shallower trend for the first 40 years (1958–1998), but it gradually recovered to be deeper recently (1998–2010). The overall spatial changes of V_s along NB suggest that the spatial pattern of NB morphology could be subdivided into two distinctive reaches, that is, N1–N12 (0–60 km), the tide-dominated reach that the volume decreases exponentially from mouth to the turning point; and N13–N16 (60–80 km), the river-tide transitional reach that the volume decreases substantially from the bifurcation to the turning point (Figure 7l).

Temporally, intertidal area reclamation, intertidal (V_i), and subtidal (V_s) volume decline was the overall trend of NB geometry change in the last 50 years. Following reclamations and the loss of intertidal area, the NB was reduced into smaller scales with concentrated channel flow. The DWS of HWL was slightly increased, and the DWS of LWL was slightly decreased, resulting in an increased tidal range of ∼30% (Figure 7j), indicating more effective channel flow due to the reduced tidal friction (Figure 7k). The concentrated and more effective channel flow was also reflected in the V_s morphology evolution that the exponential convergence trend of the tide-dominated reach became more distinct over time with geometry shrinking, that is, the reduced width in the middle and upper reach (Figure 7l). In contrast, the distribution of V_i showed no clear spatial pattern under anthropogenic reclamation and natural accretion (Figure 7m), but temporally it could be divided into two stages, that is, the first stage before 1984 when the intertidal area was wide and the total V_i was up to 1.5–1.9 km³, and the second stage after 1984 when V_i decreased dramatically by 70–80% to only ∼0.4 km³. The inconsistent change of V_s and V_i development over time in the NB reflected the difference in shoal-channel morphology evolution processes driven by intensive reclamations.

### 3.2. Intertidal Reclamation and the Subtidal Channel Response

Land reclamation, intertidal area accretion, and reclamation of the new accreted intertidal area frequently occurred over the past 50 years (Figure 7). Land reclamations were observed to occur every 5–10 years throughout the study period (Figure 8a). In total, approximately 638 km² of the intertidal area was reclaimed during the last half century, accounting for 62% of the 1958 NB water area, especially before 1991 with a total reclamation area of 550 km². Anthropogenic reclamation, although took place at the intertidal area, also resulted in strong bed erosion/accretion in the subtidal channel owing to the nature recovery forces, which can be quantified via subtracting the remaining channel volume (V_t) after reclamation from the total channel volume (V_t) in the
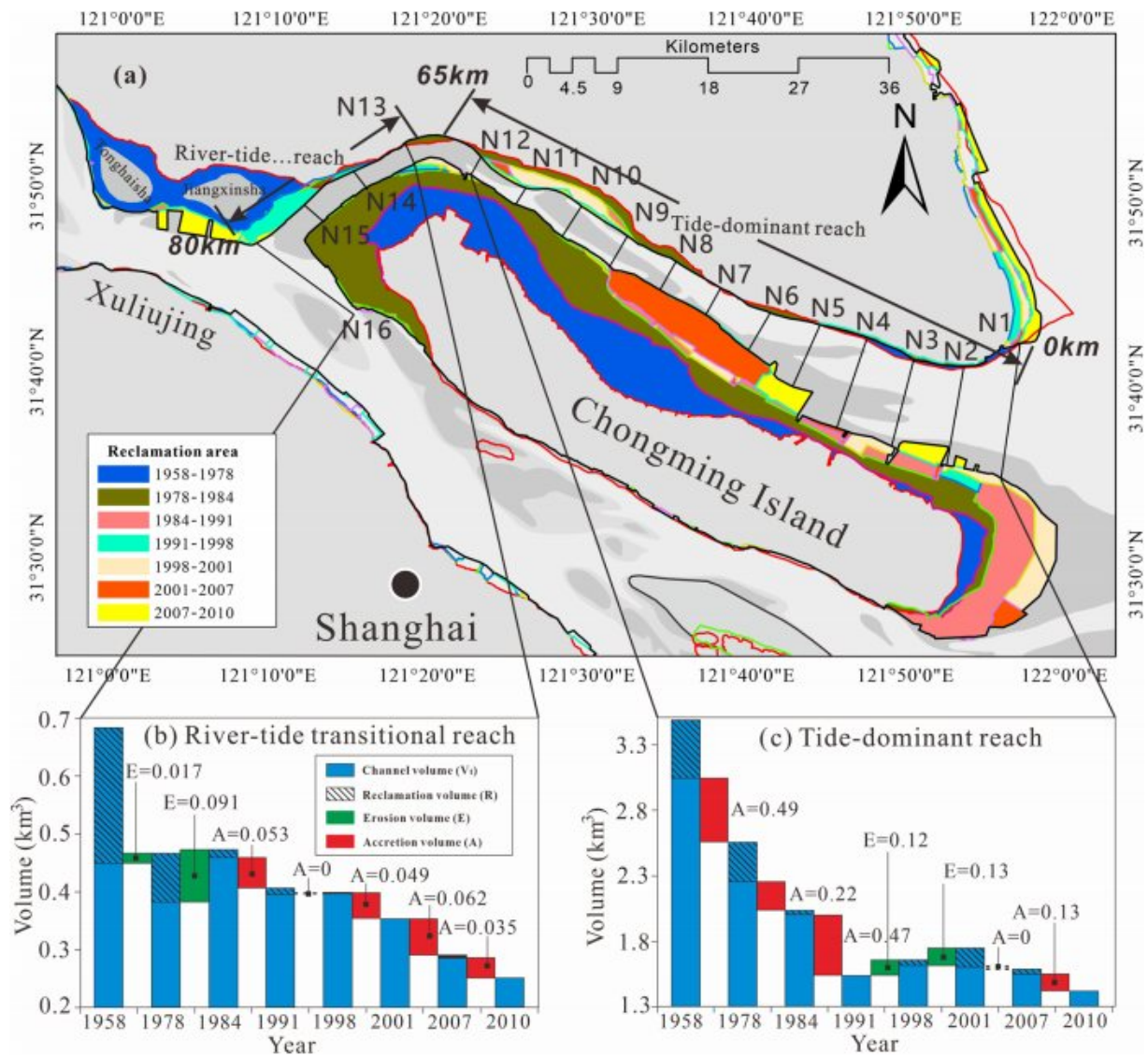
Figure 8. Historical North Branch width and volume change under reclamations. (a) The reclamation area and width change over historical periods, (b, c) total volume (V_t) change due to anthropogenic reclamation (R), natural erosion (E), and natural accretion (A) in the river-tide transitional reach and the tide-dominated reach, respectively.

following period (Figures 8b and 8c). Specifically, for the river-tide transitional reach (Figure 8b), a large channel erosion of 0.108 km^3 occurred after a significant reclamation of 0.319 km^3 during 1958–1984, which suggests a negative effect of dynamic equilibrium evolution when the channel was wide at the bifurcation. However, after 1984, a positive effect of massive channel accretion of 0.199 km^3 was triggered by a small reclamation of 0.025 km^3 in the following period 1984–2010, indicating an accelerated vanishing of channel although the reclamation works slowed down. For the tide-dominated reach (Figure 8c), a large channel accretion of 1.18 km^3 was triggered by a significant reclamation of 0.85 km^3 in 1958–1991, which suggests a positive effect of fast intertidal accretion following initial reclamations. However, after 1991, the reclamation works slowed, and erosion was dominant for the tide-dominated reach, indicating a rebound of the channel volume.

Further, reclamations of intertidal areas resulted in shrinking geometry and more constrained subtidal channels. The examined profile in the middle reach of NB (N7) illustrated the effect of reclamation on transversal morphological change in more detail (Figure 9). At the beginning of 1958, a wide intertidal and highly-curved geometry profile was observed. The southern coastline then moved seaward by 5.3, 0.8, and 0.3 km, respectively, due to the embankment of dyke building between 1958 and 1991. As a result, the intertidal area accreted consistently,
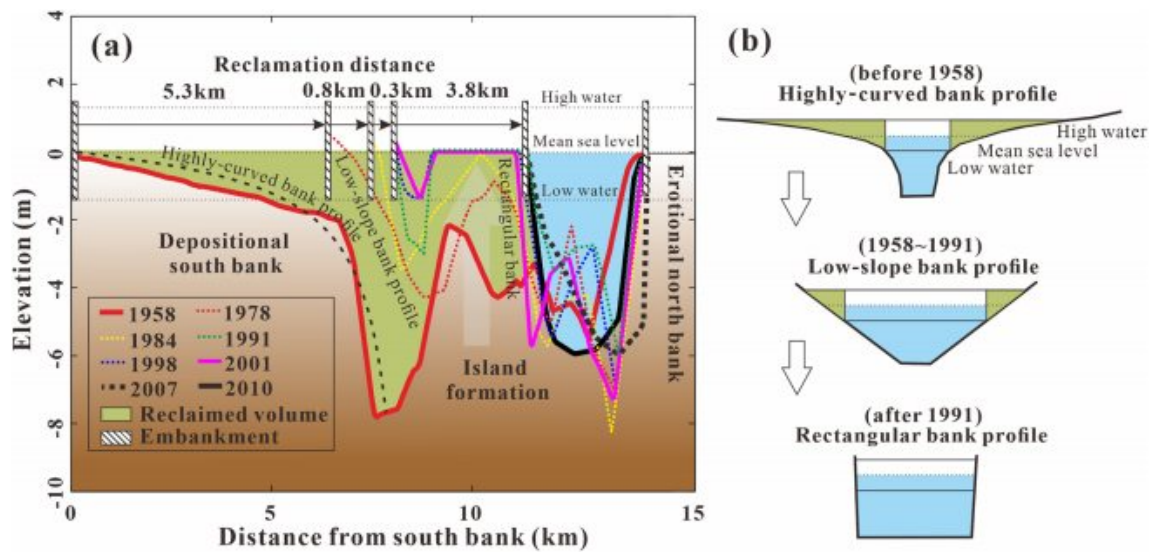
Figure 9. The channel profile variation following the reclamation procedures in the cross-section N7 from 1958 to 2010. The vertical scale of elevation is extruded by 800 times.

and the slope of the tidal front steepened fivefold from 1.3 to 6.7‰. In addition, strong sedimentation resulted in southern channel infilling and central sand island growing (Figure 9). With a substantial island reclamation in the later stages between 1991 and 2007, the coastline further transgressed by 3.8 km, and the average slope of the tidal front increased to 7.5‰. Finally, the NB changed into a highly- constrained, single-deep channel with a steep slope and embanked riparian (Figure 9). The subtidal volume was more or less maintained recently after 2001, although localized movement was observed. In addition, anthropogenic reclamation of Tonghaisha and Jiangxinsha shoals at the bifurcation (Figure 8a) directly led to the angle of NB connecting to the Changjiang River mainstream increasing from ∼45° before the 1950s to almost perpendicular after the 1970s. Consequently, the freshwater diversion ratio of about 9% in 1958 was reduced dramatically, resulting in saltwater backflow from NB to the main Changjiang River after 1978, indicating the freshwater diversion function of NB was lost after the 1970s (Dai et al., 2016).

3.3. The Predicted Future Geomorphology Evolution

Since the 2020 NB bathymetry only covers the navigation channel, the predicted future geomorphology evolution was modeled starting from the 2010 bathymetry. The NB morphology was modeled in the next 90 years without anthropogenic disturbance, assuming reclamations and other regulation works are prohibited. Under natural evolution, the shoal-channel morphology of NB showed continuous development. The intertidal area expansion and channel deepening was the overall observed trend (Figure 10). The −2, −5, and −10 m contours became straight and moved close to each other in the lower reach of the estuary, indicating the sharpening of rectangular geometry profile. Specifically, in the next 5–20 years, the intertidal area remained basically unchanged (maintained at approximately 110 km²), but the fragmented shallow shoals were gradually removed. In the next 20–40 years, the upper reach of NB was maintained, but the lower reach of the intertidal area increased profoundly with the −2 m contour moved seaward. As a result, the central bar of the south waterway evolved to be larger, potentially becoming the next generation of the branched waterway. In contrast, the deep channels of NB remained largely stable and developed to be straight in the next 20–90 years. Initially, deep channels were cut through shallow shoals in the lower reach of the estuary. The channel was then gradually deepened in the next 20 years, and sediment back-siltation was observed in the next 40 years, but the situation was converted to erosion in the next 60–90 years when the deep channel of −10 m contour extended further upstream by ∼40 km due to the gradually cleared shallow shoals at the entrance.

The channel volume (V_t) of NB decreased continuously with an infilling rate of 0.05 km³/yr according to the measured coastline and bathymetry changes from 1958 to 2010 (Figure 10f). Especially in the first 30 years from 1958 to 1991, an almost linear decline trend was observed under intensive anthropogenic reclamations.
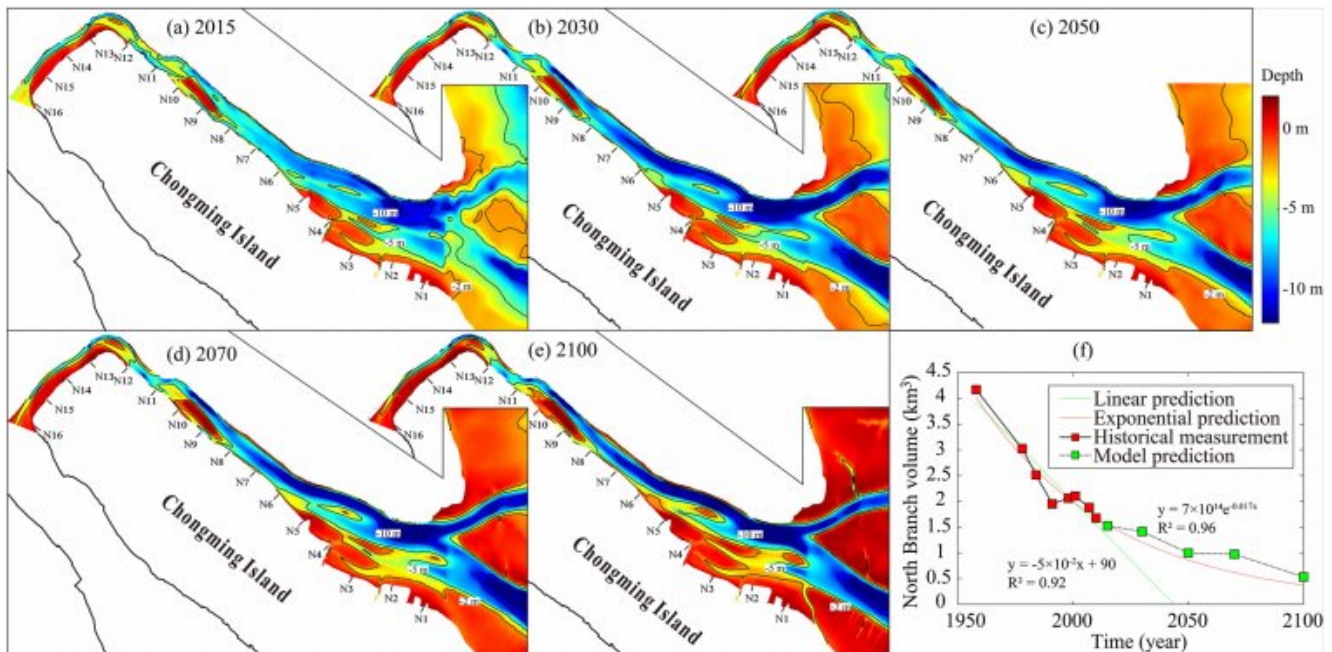
Figure 10. The predicted North Branch (NB) morphology evolution in the following decades without considering anthropogenic disturbance. (a–e) The predicted shoal-channel variations, (f) the linear and nonlinear NB volume extrapolation based on the historical measurement and the comparison with the morphodynamic modeling result.

Assuming a continuous linear infilling trend of 0.05 km^3/yr, the infilling life span of NB would be only 35 years. In other words, NB would vanish in 2045. However, according to the long-term sediment dynamics modeling, NB was not vanishing quickly over the next century. Instead, the shoal-channel morphology showed continuous development with expanding shoals and deepening channels. Therefore, the extrapolative forecasting with an exponential fitting to the historical measurement was considered a more proper trend, although it was still a little underestimating the sediment dynamics model predictions (Figure 10f). Consequently, NB morphology would persist for a long time if anthropogenic disturbances are prohibited, demonstrating the self-adjustment ability of a tide-dominated estuary after intensive reclamations. Such self-adjustment ability reflected the nonlinear geomorphological development of the large estuarine system, which was a comprehensive consequence of hydrology-morphology interactions.

3.4. System Performance Adjustment

The performance of system efficiency was evaluated in relation to energy dissipation locally and globally. In the lower reach, high energy flux demarcated two main channels, and their size and intensity were comparable in the early periods around 1958 (Figure 11a). Afterward, the energy flux asymmetry was increased, that is, the intensity in the northern channel increased while the energy flux through the southern channel decreased (Figure 11a–11f). The changes in the lower reach were compensated with energy flux variation in the upper reach. In the early periods, fragmented low-intensity energy was diffused and meandered in a wide channel (Figure 11a). More recently, the meandering flow was superseded with a single straight flow, and the high-intensity energy flux expanded further upstream to N10 (Figure 11a–11f). Integrating the energy flux over the transverse section gives the local entropy production, which indicates the distance of system efficiency from equilibrium when compared with the theoretical (exponential) energy distribution (Figure 11g). Overall, the system was moving toward equilibrium from 1958 to 1991, subsequently it varied around equilibrium (Figure 11g). More specifically, the lower (0–18 km) and upper (45–55 km) reaches showed slightly lower than equilibrium while the middle reach (18–45 km) was slightly over than equilibrium, but the distance tended to be smaller over time (Figure 11g). Such a trend was further demonstrated by showing the NB averaged residual difference (from equilibrium), that is, the system entropy production showed a linear decline from 1958 to 1991, then stayed in a relatively stable
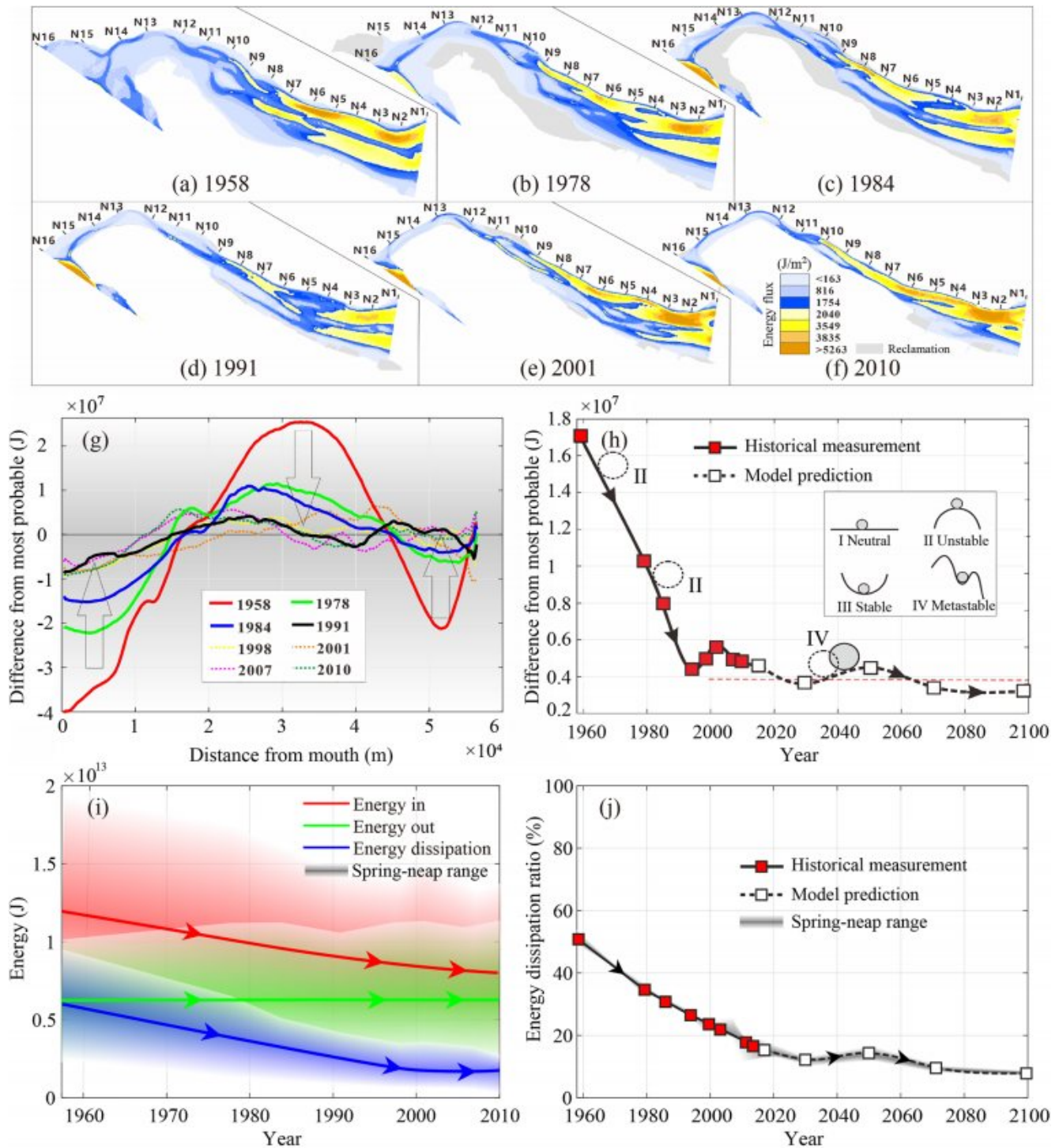
Figure 11. System efficiency variation represented by energy dissipation and entropy production. (a–f) Two-dimensional description of averaged energy flux per unit width over a tidal cycle, with the yellow color demarcating the subtidal deep channel area, (g) one-dimensional description of energy propagation along chainage of North Branch (NB) and the comparison with the theoretical most probable (exponential) energy distribution, (h) zero-dimensional description of reach averaged (N1–N12) energy flux, that is, the distance from the most probable state, in which I, II, III, and IV are neutral equilibrium, unstable equilibrium, stable equilibrium and metastable equilibrium defined by Thorn and Welford (1994), (i) variations of averaged energy into and energy out of NB and the resulted energy dissipation under spring-neap conditions, (j) energy dissipation ratio of NB for the historical measurement and future predictions, denoted with red and white square points, respectively.
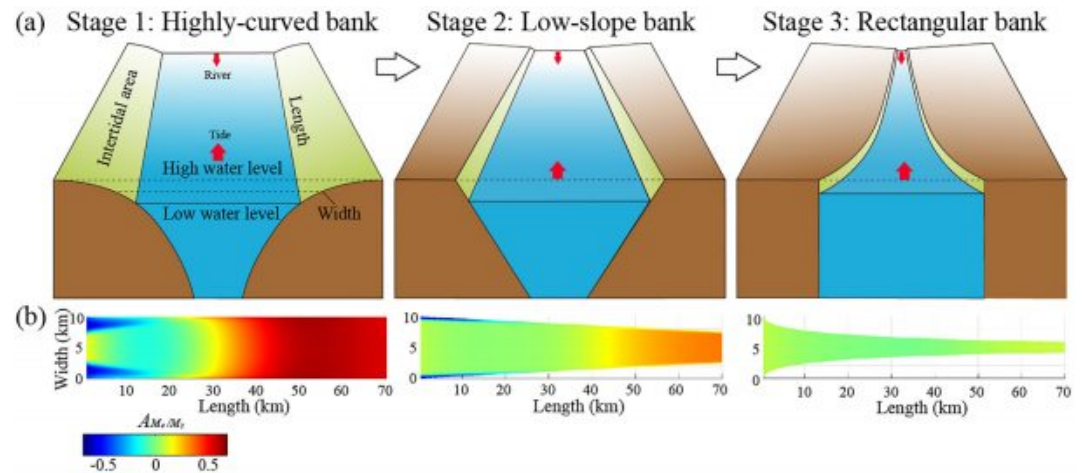
Figure 12. Prototype modeling summarizing the three stages of North Branch (NB) evolution. (a) The generalized concept model of cross-section profile describing the NB channel geometry change, (b) the modeled tidal duration asymmetry (A_{M_4/M_2}) change under the constraint of geometry and dominant forcing conditions of river and tide.

state between 1991 and 2010 (Figure 11h). The dynamic equilibrium trend continued for the predicted entropy production from 2015 to 2100 (Figure 11h).

The global energy dissipation was evaluated with the total energy entering the system from the tide and river, which declined from 1958 to 2010, while the energy exit of the system was almost constant (Figure 11i). Thus, the system energy dissipation declined over the study period. Although the system energy and energy dissipation showed large variation from spring to neap tide (>75%), the energy dissipation ratio showed slight variation (<5%), indicating a stable energy contribution to the work done globally over a tidal cycle (Figure 11j). The entropy production of the system, representing the energy dissipation to the work done locally, was also moving toward the principle of uniform energy dissipation over time (Figure 11h). Consistently, the ratio of total energy dissipation declined from 50% to 18% from 1958 to 2015, and stayed in a relative stable state over the next 90 years, meaning a gain of system efficiency of over 30% (Figure 11j). Over the same period, the system entropy production also showed fast decline from 1958 to 1991, then stayed in a relative stable state afterward (Figure 11h). Taken together these evidences, it was concluded that the NB had changed from a state of fast development to a more efficient system during the recent 10–20 years, and is expected to continue for decades. Such a stable system performance after reclamation demonstrated a state of dynamic equilibrium, or the concept of metastable equilibrium, as suggested by Thorn and Welford (1994).

4. Discussion

4.1. The NB Evolution Pattern

Reclamation procedures strongly influenced the morphology change of NB during the past 50 years. Following the intertidal reclamations, three types of geomorphologic evolution patterns were identified, which illustrated a system from preliminary estuarine shrinking to dynamic equilibrium under dominant forcing conditions of river and tide (Figure 12): **Stage 1**, the highly-curved bank channel, which is an intensive river-tide interacted system under natural condition before and around 1958. **Stage 2**, the low slope-bank channel, is a transitional form experiencing intensive anthropogenic reclamations between 1958 and 1991. **Stage 3**, the almost rectangular-bank estuary of a tidally efficient system, is a highly constrained channel of horizontally exponential convergence estuary after 1991. The bed evolution pattern of the three conceptual models was explained in relation to the tidal asymmetry effect, which mainly reflected the frictions with the subtidal and intertidal areas as demonstrated by numerical modeling (Figure 12b) and theoretical study (Friedrichs et al., 1990; Guo et al., 2018). Friction with shallow subtidal flow slows the transmission of low water, extending flood durations, while wide intertidal slows the transmission of high water, extending ebb durations (Brown & Davies, 2010; Friedrichs et al., 1990). Therefore, a highly-curved bank in Stage 1 tends to foster more flood tidal asymmetry, whereas a constant bank slope (rectangular or trapezoidal cross-section in Stages 2, 3) tends to foster less flood tidal asymmetry. The less
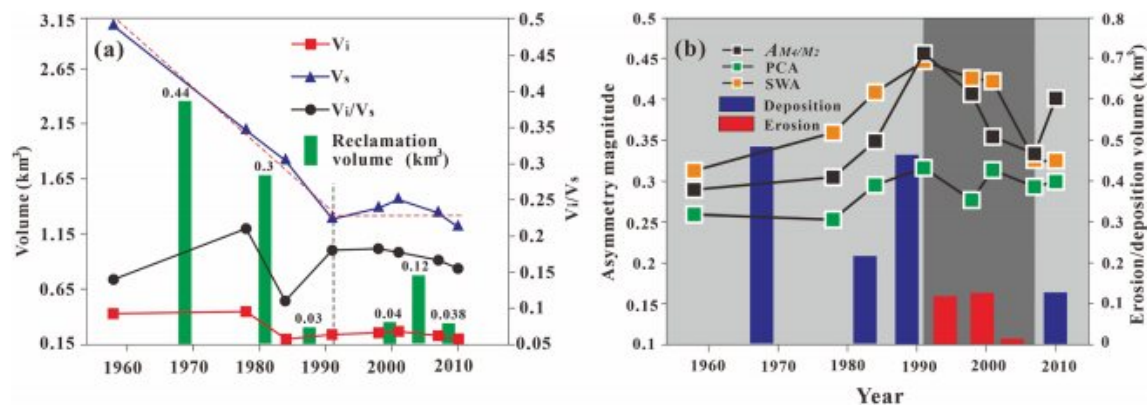
Figure 13. The hydrology-morphology adjustment of North Branch (reach N1–N12) for (a) the change of V_i, V_s, and V_i/V_s following anthropogenic reclamation, (b) the change of natural erosion and deposition following tidal duration asymmetry (A_{M_4/M_2}), peak current asymmetry (PCA), and slack water asymmetry (SWA) change. For a consistent scale, PCA and SWA are multiplied by 0.2 and 0.1, respectively.

flood-dominated estuary tends to scour and thus represents a more stable geometry (Z. B. Wang et al., 2019). The more flood-dominated estuary tends to infill the channel and therefore needs careful management (Friedrichs et al., 1990). In this case, the flood-dominated estuary of NB had become less flood tidal asymmetry from Stage 1 to Stage 2 and finally reduced to around zero in Stage 3, indicating a morphodynamic stable state (Figure 12).

Recent study by van Maren et al. (2016) discovered that land reclamation in wide shallow estuaries, like during Stage 1, would cause an increase in SSC because of the reduced accommodation volume for small-gained sediments. Given the fact that SSC has not changed (Luo et al., 2022), but the flood tidal asymmetry was strengthened after reclamation (Dai et al., 2016), it is reasonable to conclude that more sediment was transported into NB over a tidal cycle. This explained the strong accretion due to the tidal pumping effect immediately after intensive reclamations from 1958 to 1991 observed in Figure 8c. On the other hand, the asymmetry of the tide could also cause erosion if the channel was over-constrained like during Stage 3. The substantial reduction of intertidal width by reclamation could concentrate tidal current energy in the subtidal and lower intertidal space (Figure 11a–11f), with relative deep flow, resulting in bed erosion (Mariotti & Fagherazzi, 2013). A tidal flat model applied to the open estuary showed that intertidal space with a rich sediment supply could constantly accrete with a similar profile, maintaining an equilibrium condition under natural force until the channel width was too narrow to maintain an accretion state (Xie et al., 2017). The tidal current was then converted to a decreased flood asymmetry and increased erosion potential. As shown by the profile of cross-section N7 in NB (Figure 9), the southern intertidal area was progressively reduced by reclamation and increased by accretion. As a result, the front slope became steeper and finally became more vertical, and an erosional main channel occurred due to the constraint of the northern bank.

4.2. The Resilient Adjustment After Anthropogenic Disturbance

The NB evolution after anthropogenic disturbance of reclamation is mainly controlled by tidal asymmetry adjustment. Modeling of the NB hydrodynamics suggested that flood tidal asymmetry increased over time during 1958–1991 and 2007–2010 after periods of intensive intertidal reclamations in 1958–1984 and 2007, respectively, and decreased during 1991–2007 after a period of diminished intertidal reclamations during 1984–2001, due to lagged response of morphology evolution and tidal asymmetry change (Figure 13b). The higher level of flood tidal asymmetry magnitude suggested increased channel accretion and the lower level of flood tidal asymmetry magnitude suggested decreased channel accretion (Hoitink et al., 2003; Zhou et al., 2018). Moreover, reclamation of the intertidal space can strongly influence the subtidal volume evolution due to the changes in tidal asymmetry. Reclamation of the intertidal space was substantial before 1991, accounting for 1.1 km³ in total, however the V_i was almost unchanged, maintaining at around 0.43 km³, indicating a fast-growing of new intertidal space in this period (Figure 13a). The new accreted sediment not only deposited on the intertidal space but also took over the deeper part of the channel, resulted in a significant (linear) reduction of V_s from 1958 to 1991 (Figure 13a). Consequently, the NB was evolving to be narrower and shallower morphology in this period. The ratio of V_i to V_s was also fluctuating significantly between 1958 and 1991, indicating unstable and fast development of shoal-channel morphology in NB during this period. After 1991, parameters of V_i, V_s, and V_i/V_s all became more stable, with slightly decreasing V_i/V_s, indicating a deeper and narrower morphology. This trend is
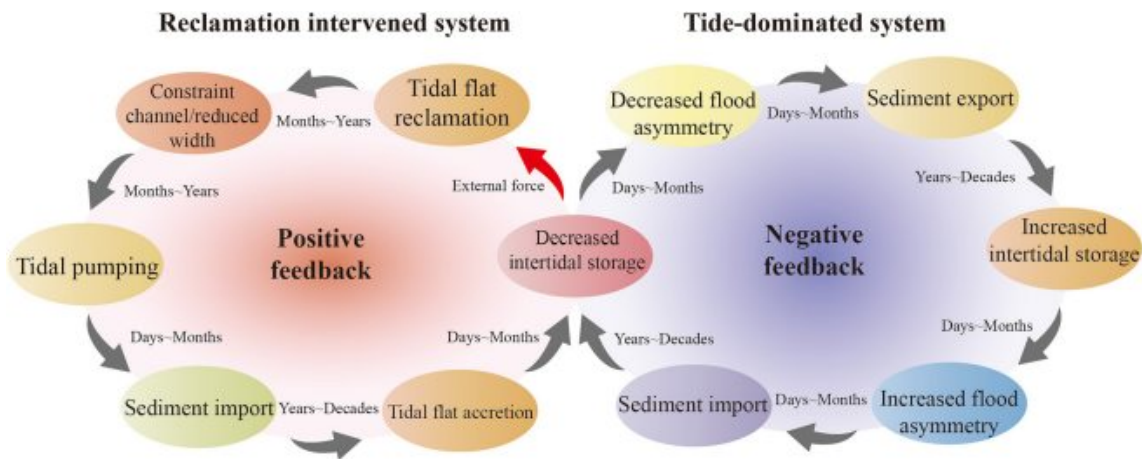
Figure 14. Equilibrium adjustment mechanism of a tide-dominated estuary under reclamations, that is, in the conversion between negative feedback loop and positive feedback loop.

closely related to changes in the level of tidal asymmetry. Hence, the growth of new intertidal space was the result of the increased level of flood tidal asymmetry, and the erosion of deep channel was the result of the decreased level of flood tidal asymmetry (Figure 13b). As a result, the inconsistent development of intertidal and subtidal volumes in the period between 1958 and 1991 had become more consistent development after 1991 (Figure 13a).

The tidal asymmetry adjustment following the three stages of NB morphology evolution demonstrated a resilient geomorphological adjustment mechanism of the tide-dominated system (Fagherazzi, 2008; Zhou et al., 2017), which moved NB evolving from preliminary estuarine shrinking to dynamic equilibrium, mainly determined by two inversive processes (Figure 14). On the one hand, anthropogenic reclamation was the main driver of estuary evolution before 1990s, forming a positive feedback on the estuarine shrinking of NB (X. Zhang, Fagherazzi, et al., 2018), that is, such an evolution loop was triggered by reclamations of the bifurcation and the lateral area, which reduced the diverted river discharge to NB, increasing the flood tidal asymmetry, thus more sediment from the ocean was transported through tidal pumping effect, causing new intertidal area accretion which were later used for reclamation (M. Zhang et al., 2021), resulted in the accelerated decline of estuary (Figure 14). On the other hand, the formation of an exponential convergence tide-dominated estuary changed the evolution loop to a negative feedback process, which was more sustainable through bed erosion following the change of tidal asymmetry (Zhou et al., 2018), especially for a large estuary, can sustain the system for quite a long time (Figure 14). The tidal asymmetry adjustment was considered as the controlling factor determined the conversion between positive feedback loop and negative feedback loop (Z. B. Wang et al., 2019). Modeling of historical hydro-sediment dynamics revealed that before massive anthropogenic interventions in Stage 1, the bank slope of NB was highly curved (Figure 9), tidal asymmetry magnitude increased, and the asymmetry phase decreased with reclamation, indicating increased flood dominance and therefore increased flood-to-ebb near-bed transport ratio, accretion of intertidal was observed (Figure 13b). Numerical modeling for NB after 1991 suggested flood-dominated system in a relative constant bank slope (Figure 9). In this condition, the asymmetry magnitude decreases with reclamation, the existing sense of tidal distortion was weakened (Figure 13b), the rate of intertidal accretion was reduced, and subtidal flushing was enhanced (Figure 9a).

4.3. The Effects of River and Tide on NB Evolution

The relative importance of river and tide on NB evolution is determined by the contribution of sediment flux, which is a function of SSC and water flux (Fagherazzi & Priestas, 2010; Xie et al., 2017). During the study period, the WD from the Changjiang River catchment was relatively stable, but the river-delivered sediment decreased significantly after the 1980s (Figure 15a). An initial assumption was that the total sediment delivery to the NB would reduce and the NB morphodynamics would change from deposition to dramatic erosion as a result of sediment deficit (Shi, 2010). However, the detailed examination of the water diversion ratio of NB (Figure 15b) demonstrated that the decreased river sediment did not have a direct impact on the NB morphology evolution. Because the water diversion function of NB was lost after 1978 (the diversion ratio reduced from 9% in 1958 to saltwater backflow), which was before the dramatic decrease of river sediment supply in 1985 (Figure 15b). The restricted water diversion from the Yangtze River turned the NB from a river-tide interacted
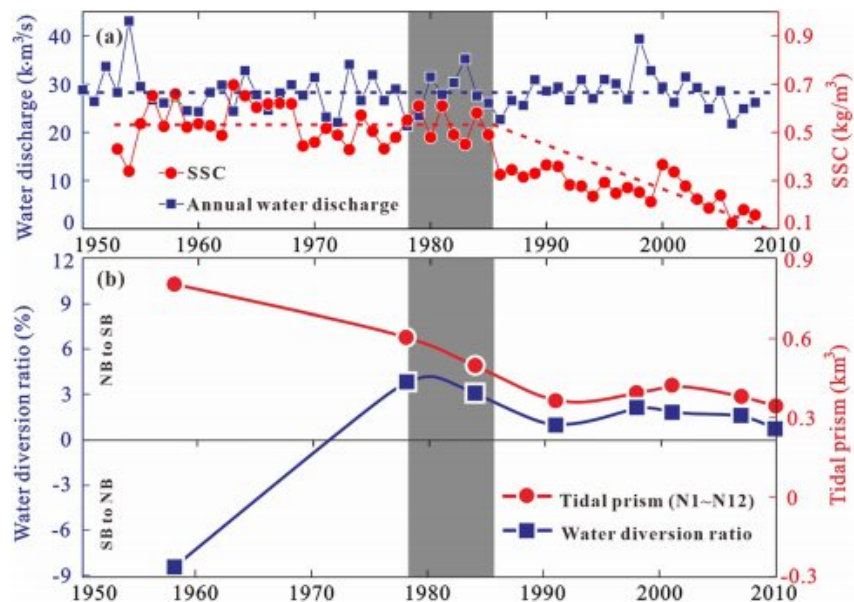
Figure 15. The comparison of riverine Sediment Discharge (SD) and water diversion ratio. (a) Annual water and SD measured at Datong station, (b) the correlation between North Branch (NB) tidal prism (from the ocean) and water diversion ratio (from the upstream), negative means the diversion of Yangtze River discharge to NB, and positive means the backflow from NB to Yangtze River main flow.

reach into a complete tide-dominated reach. As a result, the major sediment supply to the NB had changed from both river-ocean sources to a single source from the ocean due to the restricted river flow and increased tidal flow.

The restriction of water diversion from the Yangtze River could also favor NB accretion due to the tide pumping effect (Figure 14). Because when the bifurcation was blocked, the large river flood was unable to flush sediment to the ocean and the tidal pumping of deposition was enhanced, favoring sediment import to the estuary from the sea. Moreover, the maximum turbidity zone in the mouth bar of the Yangtze Estuary was unchanged in the last few decades, functioning as a new suspended sediment source (Leonardi et al., 2021). Recent research showed that the SSC in the maximum turbidity zone has not decreased despite the decreased sediment supply from upstream (Leonardi et al., 2021; Luo et al., 2022), only some net erosion and sediment coarsening were recorded (Dai et al., 2014). The formation of exponential convergence geometry in the NB would further favor tidal pumping by the increased tidal asymmetry (Zhou et al., 2018). Although the TP was reduced to a smaller degree after the 1980s due to the reduced intertidal volume under lateral reclamation (D'Alpaos et al., 2010), the water diversion at upstream was also reduced (Figure 15b). The reduced river sediment supply was compensated by the increased sediment supply from the ocean, driven by intensive tidal current. A similar process was also reported in the Ord-river estuary, Australia, that discharge regulation by river dams had triggered rapid accretion of the tidal pumping effect (Wolanski et al., 2001). Because the river dams had suppressed regular large river floods of the flushing effect, thus favoring tidal pumping of sediments into the estuary from the sea.

4.4. Implications for Future Evolution

The fate of NB was predicted to be vanished in the future (J. Chen et al., 1979; Dai et al., 2016). According to the vanishing trajectory of past shoal islands in the old Yangtze Estuary, the historical positions of Dongyin shoal, Haimen shoal, and Qidong shoal moved southeastward in 1700–1920 with a statistical attaching speed of 135 m/yr (J. Chen et al., 1979) (Figure 1b). In contrast, the human-influenced attaching speed of modern Chongming Island was estimated to be 204 m/yr between 1958 and 2010. Therefore, the impact of anthropogenic interventions on the NB vanishing was estimated to be one-third faster than the past coastline accretion speed. The vanishing of NB was an inevitable historical evolution trend, which frequently occurred over decades to centuries. Paleogeography study demonstrated at least six important periods of shoal attachment to the northern bank were identified throughout the past two thousand years (J. Chen et al., 1979). For instance, in the 6th century, Guazhou shoal, approximately 200 km from the modern estuary, was attached to the northern bank; later, in the 7th, 15th, 17th, 19th, and 1920s, Matuo shoal, Changyin shoal, Dongyin shoal, Haimen shoal,

Qidong shoal were attached, respectively (Figure 1b). Now, the new shoal islands of the Yangtze Estuary had moved to the Chongming Island. Following such a historical evolution trend, Chongming Island is predicted to attach to the northern bank by vanishing the NB, but the timescale needed will be long for such a dynamic system.

In general, land reclamations have been a common practice in estuaries (van Maren et al., 2016; W. Wang et al., 2014; M. Zhang et al., 2021). Many studies reported increasing sedimentation after reclamation (Dai et al., 2016; Fagherazzi and Priestas, 2010; van Maren et al., 2016). Assuming the linear infilling trend of 0.05 km^3/yr continues based on the historical regression analysis from 1958 to 2010, the infilling life span of NB would be only ∼35 years (Figure 10f). In other words, NB would be expected to vanish in 2045, similar to the vanishing year of 2040 estimated by Yun (2004) and is a little earlier than 2060 calculated by Dai et al. (2016). However, as the first-order distributary of the Yangtze River delta, we argued that the lifespan of NB would be longer, partly because of its large spatial scale and, more importantly, because of the resilient adjustment via complex tidal hydrodynamics and sediment transport behavior. When land reclamations altered the channel geometry, the tidal asymmetry distortion and the resulting sediment transport patterns were altered consistently (Friedrichs et al., 1990). In the NB, the evolution model switched from deposition to erosion when the channel geometry changed from a highly-curved bank to a constant-slope bank after reclamation. Moreover, low energy dissipation, minimum entropy production, and a stable state of V_i/V_s ratio were achieved in the recent 20 years instead of a rapid decline in the first 30 years, indicating a dynamic equilibrium state of NB. Further adjustment after 2010 is expected, and the model results suggest that NB will maintain a highly efficient system following exponential channel volume decrease under the estuarine preservation policies (W. Wang et al., 2014).

5. Conclusions

The long-term morphological evolution of tide-dominated estuaries under intensive anthropogenic interventions has received wide attention. When the natural evolutions are disturbed, the response processes may vary depending on their boundary and forcing conditions. The NB of Yangtze Estuary has experienced distinct morphological shrinking under anthropogenic interventions during the past 50 years, thus attracting great concern for its evolutionary fate. Here, the morphological change history and future evolution trend of NB were analyzed under dominant forcing conditions, and we tried to disentangle whether the morphodynamics was controlled by reclamation works at the local scale or boundary condition changes in the surrounding environment, such as decreased sediment supply from upstream or changing river-tide hydrodynamics. The results of hydro-morphodynamic modeling and system efficiency analysis showed the preliminary fast shrinking of NB was due to local reclamation works, but then it was transferred to a dynamic equilibrium state during the recent 20 years owing to the geomorphological resilience of a large, tide-dominated system. The morphological equilibrium and adjustment of the large system will last for a long time if preservation policies are implemented.

Notably, reclamation works at the bifurcation of Yangtze Estuary during the 1960s reduced the flow diversion ratio of NB, thus turning the NB from a river-tide interacted distributary into a complete tide-dominated distributary. The lateral reclamations of the intertidal area in the NB reduced TP and increased flood tidal asymmetry, the new accreted sediment not only deposited on the intertidal space but also took over the deeper part of the channel, leading to constrained channel flows and promoting tidal pumping. The positive feedback between reclamation and tidal deposition dominated the morphodynamic evolution of NB in the first 30 years, resulting in a significant (linear) reduction of channel volume by 55%. In contrast, during the last 20 years, the geometry of NB has changed from a highly-curved profile (with a horizontally rectangular shape) to a highly-constrained channel (with a horizontally convergent shape). The change of tidal asymmetry and the resulted sediment transport pattern had been altered from a depositional mode to an erosional mode, favoring the formation of negative feedback. Such nonlinear feedback between bathymetry, tidal asymmetry, and sediment transport drove the entire estuary toward a new morphological equilibrium. The proposed geomorphological resilience adjustment mechanism of a tide-dominated system may be relevant to other estuarine and coastal areas worldwide, which are subject to large-scale reclamations.

Conflict of Interest

The authors declare no conflicts of interest relevant to this study.

Data Availability Statement

The navigation charts covering North Branch and the surrounding area were collected from the Maritime Survey Bureau of Shanghai, Ministry of Communications of China (X. Zhang, Townend, et al., 2019), available at the website www.cccc-sdc.com. The navigation charts covering the lower reach of the Yangtze River were collected from the Changjiang Waterway Bureau, Ministry of Communications of China (X. Zhang, Townend, et al., 2019), available at the website www.cjhdj.com.cn. The bathymetry data covering the continental shelf area were collected from the GEBCO database (General Bathymetric Chart of the Oceans) (Ward, 2010). Historical coastlines were interpreted from archived TM/ETM satellite images, available at the website http://earthexplorer.usgs.gov. The daily water and SD collected at the Datong station was provided by the Changjiang Water Resources Commission (X. Zhang, Townend, et al., 2019), available at the website http://www.cjh.com.cn/. Tidal constituents were generated by TPXO 7.2 (TOPEX/POSEIDON global tidal model data set) (Egbert & Erofeeva, 2002). ArcGIS10.1 (ESRI, 2010) was used to identify the coastline movement, calculate the reclamation area, and produce spatial-temporal maps. The hydrodynamic flow was generated by TELEMAC7.1 (Hervouet, 2007). The mud transport process was generated by MIKE21FM of MIKE software 2016 (DHI, 2016), under the license provided by Shanghai Normal University. Figures were made with Matlab version 2020 (MathWorks, 2020) under the license provided by East China Normal University. Field measurement of flow direction, flow velocity, and SSC was detected with an acoustic doppler current profiler (SonTek-500), direct-read current meters (SLC9-2), and OBS-3A (5 MHz) provided by State Key Laboratory of Estuarine and Coastal Research, East China Normal University.

References

Brown, J. M., & Davies, A. G. (2010). Flood/ebb tidal asymmetry in a shallow sandy estuary and the impact on net sand transport. *Geomorphology*, *114*(3), 431–439. https://doi.org/10.1016/j.geomorph.2009.08.006

Cai, H., Savenije, H. H. G., & Gisen, J. I. A. (2016). A coupled analytical model for salt intrusion and tides in convergent estuaries. *Hydrological Sciences Journal*, *61*(2), 402–419. https://doi.org/10.1080/02626667.2015.1027206

Chen, J., Caixing, Y., Haigen, X., & Yougfa, D. (1979). The developmental model of the Changjiang River estuary during last 2000 years (in Chinese with English abstract). *Acta Oceanologica Sinica*, *01*(01), 103–111.

Chen, X., Yan, Y., Fu, R., Dou, X., & Zhang, E. (2008). Sediment transport from the Yangtze River, China, into the sea over the Post-Three Gorge Dam Period: A discussion. *Quaternary International*, *186*(1), 55–64. https://doi.org/10.1016/j.quaint.2007.10.003

Church, J. A., White, N. J., Coleman, R., Lambeck, K., & Mitrovica, J. X. (2004). Estimates of the regional distribution of sea level rise over the 1950–2000 period. *Journal of Climate*, *17*(13), 2609–2625. https://doi.org/10.1175/1520-0442(2004)017<2609:eotrdo>2.0.co;2

Dai, Z., Fagherazzi, S., Mei, X., Chen, J., & Meng, Y. (2016). Linking the infilling of the North Branch in the Changjiang (Yangtze) estuary to anthropogenic activities from 1958 to 2013. *Marine Geology*, *379*, 1–12. https://doi.org/10.1016/j.margeo.2016.05.006

Dai, Z., Liu, J. T., Wei, W., & Chen, J. (2014). Detection of the three Gorges dam influence on the Changjiang (Yangtze River) submerged delta. *Scientific Reports*, *4*(6600), 1–7. https://doi.org/10.1038/srep06600

Dai, Z., Mei, X., Darby, S. E., Lou, Y., & Li, W. (2018). Fluvial sediment transfer in the Changjiang (Yangtze) river-estuary depositional system. *Journal of Hydrology*, *566*, 719–734. https://doi.org/10.1016/j.jhydrol.2018.09.019

D'Alpaos, A., Lanzoni, S., Marani, M., & Rinaldo, A. (2010). On the tidal prism–channel area relations. *Journal of Geophysical Research*, *115*(F1), F01003. https://doi.org/10.1029/2008jf001243

Dalrymple, R. W., & Choi, K. (2007). Morphologic and facies trends through the fluvial–marine transition in tide-dominated depositional systems: A schematic framework for environmental and sequence-stratigraphic interpretation. *Earth-Science Reviews*, *81*(3–4), 135–174. https://doi.org/10.1016/j.earscirev.2006.10.002

DHI. (2016). DHI-Mike21: March 1, 2016 release (version 2016) [Software]. DHI. Retrieved from www.dhigroup.com

Dronkers, J. (1986). Tidal asymmetry and estuarine morphology. *Netherlands Journal of Sea Research*, *20*(2), 117–131. https://doi.org/10.1016/0077-7579(86)90036-0

Du, J., Shen, J., Zhang, Y. J., Ye, F., Liu, Z., Wang, Z., et al. (2018). Tidal response to sea-level rise in different types of estuaries: The importance of length, bathymetry, and geometry. *Geophysical Research Letters*, *45*(1), 227–235. https://doi.org/10.1002/2017gl075963

Egbert, G. D., & Erofeeva, S. Y. (2002). Efficient inverse modeling of barotropic ocean tides [Dataset]. Journal of Atmospheric and Oceanic Technology, *19*(2), 183–204. https://doi.org/10.1175/1520-0426(2002)019<0183:eimobo>2.0.co;2

ESRI. (2010). ArcGIS desktop: April 21, 2010 release (version 10.1.0) [Software]. ESRI. Retrieved from www.esri.com

Fagherazzi, S. (2008). Self-organization of tidal deltas. *Proceedings of the National Academy of Sciences*, *105*(48), 18692–18695. https://doi.org/10.1073/pnas.0806668105

Fagherazzi, S., & Priestas, A. M. (2010). Sediments and water fluxes in a muddy coastline: Interplay between waves and tidal channel hydrodynamics. *Earth Surface Processes and Landforms*, *35*(3), 284–293. https://doi.org/10.1002/esp.1909

Friedrichs, C. T., Aubrey, D. G., & Speer, P. E. (1990). Impacts of relative sea-level rise on evolution of shallow estuaries. In R. T. Cheng (Ed.), *Residual currents and long-term transport. Coastal and estuarine studies* (Vol. 38, pp. 105–122). Springer.

Gao, G. D., Wang, X. H., & Bao, X. W. (2014). Land reclamation and its impact on tidal dynamics in Jiaozhou Bay, Qingdao, China. *Estuarine, Coastal and Shelf Science*, *151*, 285–294. https://doi.org/10.1016/j.ecss.2014.07.017

Gao, S. (2013). Holocene shelf-coastal sedimentary systems associated with the Changjiang River: An overview. *Acta Oceanologica Sinica*, *32*(12), 4–12. https://doi.org/10.1007/s13131-013-0390-5

Guo, L., Brand, M., Sanders, B. F., Foufoula-Georgiou, E., & Stein, E. D. (2018). Tidal asymmetry and residual sediment transport in a short tidal basin under sea level rise. *Advances in Water Resources*, *121*, 1–8. https://doi.org/10.1016/j.advwatres.2018.07.012

Guo, L., Xie, W., Xu, F., Wang, X., Zhu, C., Meng, Y., et al. (2022). A historical review of sediment export–import shift in the North Branch of Changjiang Estuary. *Earth Surface Processes and Landforms*, *47*(1), 5–16. https://doi.org/10.1002/esp.5084

Hervouet, J. M. (2007). Hydrodynamics of free surface flows: Modelling with the finite element method [Software]. John Wiley & Sons, INC, New York. Retrieved from http://opentelemac.org/

Hoitink, A. J. F., Hoekstra, P., & Van Maren, D. S. (2003). Flow asymmetry associated with astronomical tides: Implications for the residual transport of sediment. *Journal of Geophysical Research*, *108*(C10), 3315. https://doi.org/10.1029/2002jc001539

Hoitink, A. J. F., Wang, Z. B., Vermeulen, B., Huismans, Y., & Kästner, K. (2017). Tidal controls on river delta morphology. *Nature Geoscience*, *10*(9), 637–645. https://doi.org/10.1038/ngeo3000

Kuang, C., Chen, K., Wang, J., Wu, Y., Liu, X., & Xia, Z. (2021). Responses of hydrodynamics and saline water intrusion to Typhoon Fongwong in the North Branch of the Yangtze River estuary. *Applied Sciences*, *11*(19), 8986. https://doi.org/10.3390/app11198986

Leonardi, N., Mei, X., Carnacina, I., & Dai, Z. (2021). Marine sediment sustains the accretion of a mixed fluvial-tidal delta. *Marine Geology*, *438*, 106520. https://doi.org/10.1016/j.margeo.2021.106520

Li, Z., Li, M. Z., Dai, Z., Zhao, F., & Li, J. (2015). Intratidal and neap-spring variations of suspended sediment concentrations and sediment transport processes in the North Branch of the Changjiang Estuary. *Acta Oceanologica Sinica*, *34*(1), 137–147. https://doi.org/10.1007/s13131-015-0605-z

Luan, H. L., Ding, P. X., Wang, Z. B., & Ge, J. Z. (2017). Process-based morphodynamic modeling of the Yangtze Estuary at a decadal timescale: Controls on estuarine evolution and future trends. *Geomorphology*, *290*, 347–364. https://doi.org/10.1016/j.geomorph.2017.04.016

Luan, H. L., Ding, P. X., Wang, Z. B., Ge, J. Z., & Yang, S. L. (2016). Decadal morphological evolution of the Yangtze Estuary in response to river input changes and estuarine engineering projects. *Geomorphology*, *265*, 12–23. https://doi.org/10.1016/j.geomorph.2016.04.022

Luo, W., Shen, F., He, Q., Cao, F., Zhao, H., & Li, M. (2022). Changes in suspended sediments in the Yangtze River Estuary from 1984 to 2020: Responses to basin and estuarine engineering constructions. *Science of The Total Environment*, *805*, 150381. https://doi.org/10.1016/j.scitotenv.2021.150381

Mariotti, G., & Fagherazzi, S. (2013). A two-point dynamic model for the coupled evolution of channels and tidal flats. *Journal of Geophysical Research: Earth Surface*, *118*(3), 1387–1399. https://doi.org/10.1002/jgrf.20070

MathWorks. (2020). MATLAB R2020a (version 9.8.0) [Software]. MathWorks. Retrieved from www.mathworks.com

Mei, X., Dai, Z., Darby, S. E., Zhang, M., Cai, H., Wang, J., & Wei, W. (2021). Landward shifts of the maximum accretion zone in the tidal reach of the Changjiang estuary following construction of the Three Gorges Dam. *Journal of Hydrology*, *592*, 125789. https://doi.org/10.1016/j.jhydrol.2020.125789

Mi, J., Zhang, M., Zhu, Z., Vuik, V., Wen, J., Gao, H., & Bouma, T. J. (2022). Morphological wave attenuation of the nature-based flood defense: A case study from Chongming Dongtan Shoal, China. *Science of the Total Environment*, *831*, 154813.

Nienhuis, J. H., Ashton, A. D., Edmonds, D. A., Hoitink, A. J. F., Kettner, A. J., Rowland, J. C., & Törnqvist, T. E. (2020). Global-scale human impact on delta morphology has led to net land area gain. *Nature*, *577*(7791), 514–518. https://doi.org/10.1038/s41586-019-1905-9

Partheniades, E. (1965). Erosion and deposition of cohesive soils. *Journal of Hydraulic Engineering*, *91*(1), 105–139. https://doi.org/10.1061/jyceaj.0001165

Sheng, J., Rui, D., & Han, X. (2022). Governmentality and sociotechnical imaginary within the conservation-development nexus: China's great Yangtze River protection programme. *Environmental Science & Policy*, *136*, 56–66. https://doi.org/10.1016/j.envsci.2022.05.018

Shi, J. Z. (2010). Tidal resuspension and transport processes of fine sediment within the river plume in the partially-mixed Changjiang River estuary, China: A personal perspective. *Geomorphology*, *121*(3), 133–151. https://doi.org/10.1016/j.geomorph.2010.04.021

Smagorinsky, J. (1963). General circulation experiments with the primitive equations: I. The basic experiment. *Monthly Weather Review*, *91*(3), 99–164. https://doi.org/10.1175/1520-0493(1963)091<0099:gcewtp>2.3.co;2

Sternberg, R. W., Berhane, I., & Ogston, A. (1999). Measurement of size and settling velocity of suspended aggregates on the northern California continental shelf. *Marine Geology*, *154*(1), 43–53. https://doi.org/10.1016/s0025-3227(98)00102-9

Syvitski, J. P. M., Kettner, A. J., Overeem, I., Hutton, E. W. H., Hannon, M. T., Brakenridge, G. R., et al. (2009). Sinking deltas due to human activities. *Nature Geoscience*, *2*(10), 681–686. https://doi.org/10.1038/ngeo629

Thorn, C. E., & Welford, M. R. (1994). The equilibrium concept in geomorphology. *Annals of the Association of American Geographers*, *84*(4), 666–696. https://doi.org/10.1111/j.1467-8306.1994.tb01882.x

Townend, I. (2012). The estimation of estuary dimensions using a simplified form model and the exogenous controls. *Earth Surface Processes and Landforms*, *37*(15), 1573–1583. https://doi.org/10.1002/esp.3256

Townend, I., & Dun, R. (2000). A diagnostic tool to study long-term changes in estuary morphology. *Geological Society, London, Special Publications*, *175*(1), 75–86. https://doi.org/10.1144/gsl.sp.2000.175.01.07

van der Wegen, M., Wang, Z. B., Savenije, H. H. G., & Roelvink, J. A. (2008). Long-term morphodynamic evolution and energy dissipation in a coastal plain, tidal embayment. *Journal of Geophysical Research*, *113*(F3), F3001.

van Maren, D. S., Oost, A., Wang, Z., & Vos, P. (2016). The effect of land reclamations and sediment extraction on the suspended sediment concentration in the Ems Estuary. *Marine Geology*, *376*, 147–157. https://doi.org/10.1016/j.margeo.2016.03.007

Wang, W., Liu, H., Li, Y., & Su, J. (2014). Development and management of land reclamation in China. *Ocean & Coastal Management*, *102*, 415–425. https://doi.org/10.1016/j.ocecoaman.2014.03.009

Wang, X., Xiao, X., Xu, X., Zou, Z., Chen, B., Qin, Y., et al. (2021). Rebound in China's coastal wetlands following conservation and restoration. *Nature Sustainability*, *4*(12), 1076–1083. https://doi.org/10.1038/s41893-021-00793-5

Wang, Y., Dong, P., Oguchi, T., Chen, S., & Shen, H. (2013). Long-term (1842–2006) morphological change and equilibrium state of the Changjiang (Yangtze) Estuary, China. *Continental Shelf Research*, *56*, 71–81. https://doi.org/10.1016/j.csr.2013.02.006

Wang, Z. B., Vandenbruwaene, W., Taal, M., & Winterwerp, H. (2019). Amplification and deformation of tidal wave in the Upper Scheldt Estuary. *Ocean Dynamics*, *69*(7), 829–839. https://doi.org/10.1007/s10236-019-01281-3

Ward, R. (2010). General bathymetric chart of the oceans [Dataset]. *Hydro International*, *14*(5), 45. Retrieved from www.gebco.net

Wei, W., Dai, Z., Mei, X., Liu, J. P., Gao, S., & Li, S. (2017). Shoal morphodynamics of the Changjiang (Yangtze) estuary: Influences from river damming, estuarine hydraulic engineering and reclamation projects. *Marine Geology*, *386*, 32–43. https://doi.org/10.1016/j.margeo.2017.02.013

Wolanski, E., Moore, K., Spagnol, S., D'Adamo, N., & Pattiaratchi, C. (2001). Rapid, human-induced siltation of the macro-tidal Ord river estuary, Western Australia. *Estuarine, Coastal and Shelf Science*, *53*(5), 717–732. https://doi.org/10.1006/ecss.2001.0799

Xie, D., Pan, C., Wu, X., Gao, S., & Wang, Z. B. (2017). Local human activities overwhelm decreased sediment supply from the Changjiang River: Continued rapid accumulation in the Hangzhou Bay-Qiantang Estuary system. *Marine Geology*, *392*, 66–77. https://doi.org/10.1016/j.margeo.2017.08.013

Yu, S., Yang, J., & Liu, G. (2014). Impact assessment of Three Gorges Dam's impoundment on river dynamics in the north branch of Yangtze River estuary, China. *Environmental Earth Sciences*, *72*(2), 499–509. https://doi.org/10.1007/s12665-013-2971-1

Yun, C. X. (2004). *Evolutionary rules of the Changjiang estuary in recent decades*. China Ocean Press.

Zhang, E., Gao, S., Savenije, H. H., Si, C., & Cao, S. (2019). Saline water intrusion in relation to strong winds during winter cold outbreaks: North Branch of the Yangtze Estuary. *Journal of Hydrology*, *574*, 1099–1109. https://doi.org/10.1016/j.jhydrol.2019.04.096

Zhang, M., Dai, Z., Bouma, T. J., Bricker, J., Townend, I., Wen, J., et al. (2021). Tidal-flat reclamation aggravates potential risk from storm impacts. *Coastal Engineering*, *166*, 103868. https://doi.org/10.1016/j.coastaleng.2021.103868

Zhang, M., Townend, I., Cai, H., He, J., & Mei, X. (2018). The influence of seasonal climate on the morphology of the mouth-bar in the Yangtze Estuary, China. *Continental Shelf Research*, *153*(Supplement C), 30–49. https://doi.org/10.1016/j.csr.2017.12.004

Zhang, M., Townend, I., Zhou, Y., & Cai, H. (2016). Seasonal variation of river and tide energy in the Yangtze estuary, China. *Earth Surface Processes and Landforms*, *41*(1), 98–116. https://doi.org/10.1002/esp.3790

Zhang, M., Townend, I, Zhou, Y., Wang, L., & Dai, Z. (2019). An examination of estuary stability in response to human interventions in the South Branch of the Yangtze (Changjiang) estuary, China [Dataset]. Estuarine, Coastal and Shelf Science, *228*, 106383. https://doi.org/10.1016/j.ecss.2019.106383

Zhang, X., Fagherazzi, S., Leonardi, N., & Li, J. (2018). A positive feedback between sediment deposition and tidal prism may affect the morphodynamic evolution of tidal deltas. *Journal of Geophysical Research: Earth Surface*, *123*(11), 2767–2783. https://doi.org/10.1029/2018jf004639

Zhou, Z., Coco, G., Townend, I., Gong, Z., Wang, Z., & Zhang, C. (2018). On the stability relationships between tidal asymmetry and morphologies of tidal basins and estuaries. *Earth Surface Processes and Landforms*, *9*(43), 1943–1959. https://doi.org/10.1002/esp.4366

Zhou, Z., Coco, G., Townend, I., Olabarrieta, M., van der Wegen, M., Gong, Z., et al. (2017). Is "morphodynamic equilibrium" an oxymoron? *Earth-Science Reviews*, *165*, 257–267. https://doi.org/10.1016/j.earscirev.2016.12.002